ABSTRACT

Title of Dissertation / Thesis: EXTREME GEOTECHNICAL RESPONSE TO HIGH HEAT FROM TUNNEL FIRES

Meng Wah Yong, M.S., 2004

Dissertation / Thesis Directed By: Professor André Marshall, Department of Fire Protection Engineering; and
Professor Deborah Goodings, Department of Civil and Environmental Engineering

This study investigates the effects of heating on the *transient* behavior of the geologic media surrounding the tunnel involved in a severe fire, which typically involve extreme temperature and prolonged duration. Currently, there is little research being done in this area. An analytical model has been developed to predict the temperature rise of dry soil in the experimental soil column configuration and there is good agreement between analytical and experimental results. In water-saturated soils, the onset of convection happens in soil of higher permeability and there is propagation of a saturation temperature front at the onset of boiling, with greater propagation speed as permeability increases. There is also significant increase (~500%) in the pore water pressure building up in finer-grained saturated soil. This project then examines how these thermal transport modes and the pore water pressure increase in the soil medium can affect the stability of the tunnel lining.

EXTREME GEOTECHNICAL RESPONSE TO HIGH HEAT FROM TUNNEL FIRES

By

MENG WAH YONG

Thesis submitted to the Faculty of the Graduate School of the
University of Maryland, College Park, in partial fulfillment
of the requirements for the degree of
Master of Science
2004

Advisory Committee:
Professor André Marshall, Chair
Professor Deborah Goodings
Professor James Milke

Acknowledgements

The work presented in this Master Thesis is funded by the National Science Foundation under Grant No. 0331332.

First and foremost, I would like to express my heartfelt gratitude to Professor André Marshall and Professor Goodings for their wonderful guidance, knowledge and support, without which, all these work will not be possible.

In addition, I would like to thank two undergraduate exchange students from Germany namely Daniela Gehrig and Paul Kalinowski, and David Capka, who was a part-time graduate student from the Department of Civil Engineering. They assisted me greatly in the design and fabrication of the test apparatus as well as running the experiments.

Last but not least, I am most grateful to my wife for her understanding and enormous support during the course of my MS program.

Table of Contents

List of Tables

List of Figures

CHAPTER 1: INTRODUCTION

This chapter examines some of the previous work done and explores the potential impact to the stability of the tunnel lining due to thermally-induced pore pressure and soil movement as a result of tunnel fires. The objectives for this exploratory project and the justifications for the experimental configuration are also spelled out.

1.1 Motivation for Project

Tunnel fires typically involve extreme temperature and prolonged duration which could potentially pose catastrophic risks to the structural stability of the tunnel lining and its supporting soil structure. Studies examining the two fires of notable concern - the 1996 Channel Tunnel fire (Ulm et al., 1999) and the 2001 Baltimore Howard St Tunnel fire (McGrattan and Hamins, 2003) reported maximum temperatures as high as 800^{o}C and durations as long as 48 hours. Figure 1 shows a photo of a tunnel involved in a severe fire. Although some research has been done examining the response of concrete tunnel linings and porous media subjected to high temperature, no attention has been given to the study of the effect of such *extreme* conditions on the *transient* behavior of the geologic media surrounding the tunnel involved in a severe fire.

Figure 1. Photo showing a tunnel involved in a fire (www.etnfit.net)

Ulm et al. (1999a) and Ulm et al. (1999b) examined extensively the damage to the concrete lining in the Channel tunnel subjected directly to temperature up to 700^{o}C and rapid temperature increase. Sahota and Pagni (1979) also developed analytical solutions for heat and mass transfer in porous media subjected to fires but their results were confined to specific applications i.e. partially saturated porous media such as concrete with no movement of the liquid fluid.

Mitchell (1993) reported experimental results describing the response of saturated soils subjected to temperature up to 60^{o}C under drained and undrained conditions, where boiling phenomena was not expected. Houston et al. (1985) also investigated the stress-strain behavior of saturated soils subjected to a temperature range of 4 to 200^{o}C in a study to ascertain the geotechnical response surrounding a canister of radioactive waste buried approximately 30 m below the seafloor in deep ocean waters. However, their studies were limited to soil behaviors under steady-state and uniform temperature conditions, and there was no boiling phenomenon.

Bau and Torrance (1982) considered the Rayleigh number criterion for determining the onset of steady-state convection in a vertical cylinder filled with porous materials and heated from below. They found that the onset of convection cells occurred in porous material of higher permeability and the propensity of the onset of convection was in good agreement with the analytical prediction based on the Rayleigh number. In another separate experiment on boiling in porous media, Bau and Torrance (1982) observed the formation of an isothermal two-phase vapor and liquid region underlying a liquid phase at the onset of boiling in the soil matrix. However, their experiments, similar to Houston studies, focused on investigating soil behaviors under steady state conditions and the imposed heat flux was also comparatively less extreme (< 1 kW/m^2).

Eckert and Faghri (1980) developed analytical solutions to describe the moisture migration field with time in an unsaturated porous medium due to a temperature change. They found that the moisture field before dry-out was dependent on two dimensionless parameters i.e. Luikov and Fourier numbers only. However, their studies were limited to specific applications where (1) the temperature difference above ambient imposed on the medium was small ($\Delta T \approx 50^oC$) so that the total pressure was constant and (2) the vapor pressure was small compared to the total air pressure.

It is further observed that existing studies on the measurement of pore water pressure in soil media under uniform temperature conditions are markedly inadequate to

provide explanations on the pore pressure development subjected to severe temperature gradients characteristic of severe tunnel fires.

1.1.1 Initial Heat Transfer Analysis

Preliminary calculations were performed to ascertain the temperature conditions that could develop in the saturated soil medium surrounding a tunnel involved in a severe fire. For this analysis, it is assumed that the tunnel has a concrete lining 400mm thick surrounded by overlaying soil medium consisting of silt, clay and sand, and is involved in a severe fire. Furthermore, a Crank-Nicholson implicit finite difference 1-D heat transfer model is used to predict the fire-induced temperature rise in the concrete and soil medium exposed to a constant surface heat flux of 50 kW/m^2, using average thermal diffusivity values $\alpha_{concrete} = 7x10^{-7}m^2/s$ and $\alpha_{soil} = 5x10^{-7}m^2/s$, and assuming infinite medium boundary conditions. Figure 2 shows the results of this analysis, indicating that the temperature at the interface of the soil medium and concrete lining can rise as high as 350^oC within a short exposure time of 48 hrs. These long fire durations are common in severe tunnel fires such as the 2001 Baltimore Howard St Tunnel fire. In addition, it has been reported that the peak ceiling temperature could reach 800^oC within a relatively short time (McGrattan and Hamins, 2003) during a fully involved tunnel fire. It is then speculated that thermal spalling of concrete would occur, considering the rapid temperature rise experienced by the concrete lining (Ulm et al., 1999). If spalling occurred, the thickness of concrete lining would be reduced and the fire-induced temperature in the saturated soil medium could rise even higher. The geotechnical response to this severe

temperature gradient is unknown and remains unexplored (after extensive literature survey), and thus provides a motivation for this research project.

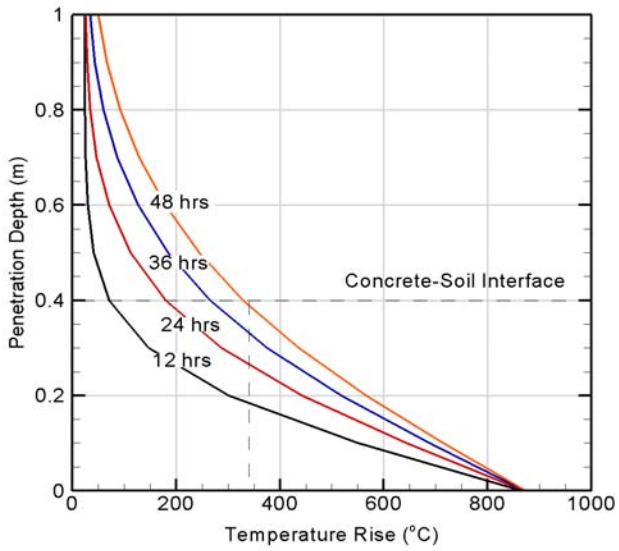

Figure 2: Fire-induced temperature rise in the soil medium surrounding a tunnel ($\dot{q}''$ =50 kW/m^2; $\alpha_{concrete}$ =7x10^{-7} m^2/s;α_{soil} =5x10^{-7} m^2/s).

1.1.2 Potential Impact Due to Pore Water Pressure and Soil Movement

According to the Tunnel Engineering Handbook (1996), the most common criteria used in the structural design of soft ground tunnel linings is based on the ability of the tunnel lining to withstand a soil load and an imposed deformation. The soil load is due to the overlaying soil medium and the groundwater pressure. The deformation criterion addresses imposed loads and is specified in terms of a certain percentage of the critical dimensions of the tunnel. It also emphasizes that the tunnel lining system leverages on controlled ground deformation to mobilize ground strength, thus continuous contact between the lining and the ground is of critical importance for the

stability of the tunnel lining. Campanella and Mitchell (1968) observed that increased temperature in saturated soils under drained condition at constant effective stress results in permanent densification of the saturated soil specimen whilst temperature rise at undrained condition could cause excess pore water pressure to build up significantly. Consequently, when subjected to high heat flux during a tunnel fire, additional load attributed to the built-up pore pressure and soil densification could develop at the crown of the tunnel lining. Excessive built-up pore pressure may also induce instantaneous stresses within the lining beyond the permissible design limit. Moreover, the pore pressure and boiling phenomena resulting from a high heat flux, cause small cavities to open and close within the soil matrix, leading to the formation of voids. If there is no continuous contact between the lining and the surrounding soil medium i.e. existence of voids, mobilizing the ground strength for tunnel stability will not be effective, thereby leading to probable failure of the tunnel lining due to large uncontrolled deformation.

Ultimately, the purpose of this research is to explore this previously overlooked area: the response and the potential impact on the soil structure surrounding a tunnel when it is subjected to the extreme heat flux accompanying severe tunnel fires.

1.2 Objectives

Keeping in mind that this project is exploratory in nature, the objectives set out for this project include:

(1) To appreciate the physics and dominant mechanisms that govern the behavior of soil subjected to extreme temperature and heat flux;

(2) To conduct experiments to investigate geotechnical response, simulating the actual physical conditions experienced during severe tunnel fires;

(3) To identify critical dimensionless parameters that characterize the expected behaviors of soils subjected to extreme temperature; and

(4) To establish qualitatively the potential impact on the stability of the tunnel linings due to specific geotechnical behaviors ensuing extreme temperature exposure.

1.3 Justifications for the Experimental Configuration

In an actual tunnel fire, it is likely that there will be non-uniformity in the excess pore water pressure development, consolidation effects and soil migration due to severe temperature gradients in the soil medium surrounding the tunnel lining. Conducting tests on isolated thin specimens with uniform temperature as in the Houston and Lin (1987) studies, will not yield realistic responses representative of actual ground conditions. As such, a 1-D experimental configuration was used to allow simple spatial variations to develop. The 1-D behavior is realized by enclosing a cylindrical core of soil, simulating a vertical column of soil medium overlaying a hemispherical tunnel as depicted in Figure 3.

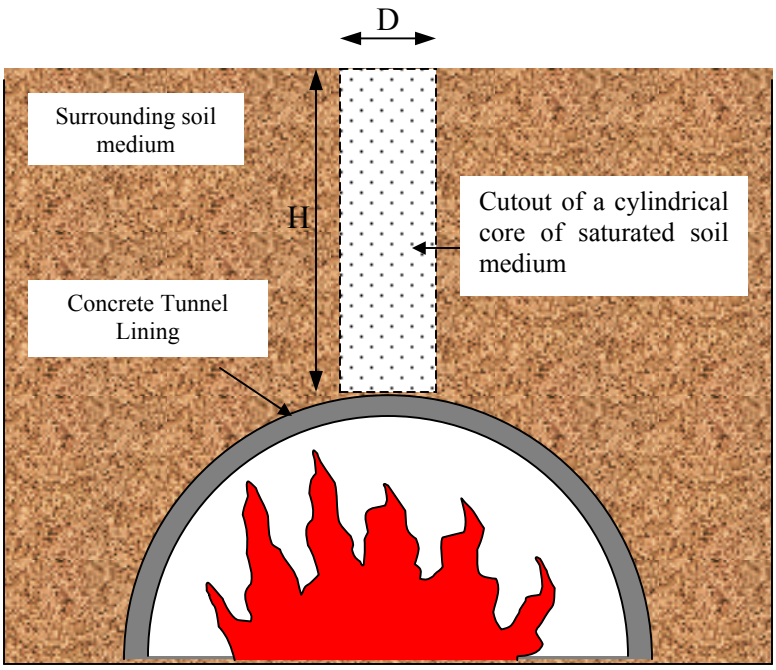

Figure 3. Experimental approach showing the cutout of a cylindrical core of saturated soil medium surrounding the tunnel involved in a fire. H:column height; D: diameter.

The top of the column is open to the ambient air and the bottom end is closed. The apparatus is watertight, except at the top of the column. A surcharge can be applied to the upper soil surface to simulate the realistic depth of soil above the tunnel lining. High heat flux is applied at the bottom of the column and the tube enclosing the soil is wrapped with adequate insulation to insure that the dominant direction of heat transfer is one-dimensional and vertical. The response of soil subjected to the high heat flux is recorded using an array of thermocouples and pressure transducers at various elevations to measure the temperatures and pore water pressures. Changes in the mechanical properties of the soil, if any, are measured from soil samples collected during the dissection of the soil column after cooling.

CHAPTER 2: LITERATURE REVIEW

This chapter looks at the extreme conditions experienced in recent major tunnel fires and the adverse consequences arising from these conditions. In order to enhance the appreciation of the physics of mass and heat transfer in porous medium heated from below, background information on the various thermal transport modes occurring in porous medium such as conduction, convection and boiling, and the mechanical response of soil at elevated temperature are discussed. In addition, the pertinent factors affecting the stability of tunnel lining are described.

2.1 Likely Extreme Conditions Experienced In Tunnel Fires

The effects of major tunnel fires cannot be understated and unfortunately, severe tunnel fires are not uncommon. On 18 Nov 1996, a fire involving a train transporting trucks in the 51 km long English Channel tunnel burned for about 10 hours and the maximum air temperature attained was estimated to be about 700^{o}C. The fire damaged several meters of the concrete tunnel lining and at certain parts of the tunnel, the thickness of the concrete lining was drastically reduced to only about 2 inches due to the severe effect of thermally-induced spalling. The Channel tunnel was closed for 6 months for repairs and the loss was estimated to be $1.5 million per day (Ulm et al, 1999a).

On 24 March 1999, a catastrophic fire occurred in the 11.6 km long Mont Blanc tunnel when a tractor-trailer carrying margarine and flour caught fire. Other vehicles

became involved in the fire relatively quickly. It burned for more than 72 hours and the maximum temperature was reported to be as high as 1000^{o}C. The average size of the fire throughout the duration was estimated to be about 30 to 50 MW but the instantaneous values could be much higher (≈100MW). Tragically, 39 people were killed in the fire. Over 900 m of the tunnel crown was also damaged due to spalling (French Task Force 1999).

In 2001, a train carrying hazardous materials (tripropylene) derailed, caught fire in the Howard St Tunnel at Baltimore, Maryland and the fire burned for more than 48 hours. A study was carried out by McGrattan and Hamins from the National Institute of Standards and Technology (NIST) under the sponsorship of the US Nuclear Regulatory Commission (NRC) to evaluate the thermal conditions in the tunnel during the fire. The modeling results from Fire Dynamics Simulator (FDS) predicted that the peak lining surface temperature and heat flux in the vicinity of the fire could reach 800^{o}C and 150 kW/m^{2} respectively. Table 1 gives a summary of the extreme conditions experienced during recent severe tunnel fires.

Table 1. Summary of the extreme conditions experienced during recent tunnel fires

Date	Location	Max Temp	Duration
1996	English Channel (between England and France)	700^{o}C	10 hrs
1999	Mont Blanc (between France and Italy)	1000^{o}C	72 hrs
2001	Howard St Tunnel	800^{o}C	48 hrs

2.2 Predominant Heat Transfer Mechanisms

The physics and governing equations for three thermal transport modes namely conduction, convection and boiling, predominant in soil medium heated from below are analyzed in this section. Furthermore, the heat and mass flow analysis of multi-phase flow in multi-components porous medium is briefly expounded.

2.2.1 Conduction Phenomena

The equation for a simple one-dimensional heat transfer via conduction through the soil column, assuming that there is negligible heat loss, is given by:

$$k\frac{\partial T}{\partial t} = \rho c_p \frac{\partial^2 T}{\partial x^2} \Rightarrow \frac{\partial T}{\partial t} = \alpha \frac{\partial^2 T}{\partial x^2} \tag{2.1}$$

where k is the thermal conductivity of the soil medium (W/m.K); ρ and c_p refer to the density (kg/m^3) and specific heat capacity (J/kg.K) of the soil medium respectively; $\alpha = k/\rho c_p$ is the thermal diffusivity of the soil medium (m^2/s). Discretization of Eqn. (2.1) allows a finite-difference model to be developed to predict the temperature rise within a dry soil column when heated from below. Crank-Nicholson method provides a numerical implicit scheme with approximations that are second-order both in time and space. The time and space derivates can be approximated as follows:-

$$\frac{\partial T}{\partial t} = \frac{T_i^{l+1} - T_i^{l}}{\Delta t} \tag{2.2}$$

and

$$\frac{\partial^2 T}{\partial x^2} = \frac{1}{2}\left(\frac{T_{i+1}{}^{l} - 2T_i^{l} + T_{i-1}{}^{l}}{(\Delta x)^2} + \frac{T_{i+1}{}^{l+1} - 2T_i^{l+1} + T_{i-1}{}^{l+1}}{(\Delta x)^2} \right) \tag{2.3}$$

Substituting Eqns (2.2) and (2.3) into Eqn. (2.1) and consolidating the terms gives:

$$-\gamma T_{i-1}^{\,l+1} + 2(1+\gamma)T_i^{\,l+1} - \gamma T_{i+1}^{\,l+1} = \gamma T_{i-1}^{\,l} + 2(1-\gamma)T_i^{\,l} + \gamma T_{i+1}^{\,l} \qquad (2.4)$$

where $\gamma = \dfrac{\alpha \Delta t}{(\Delta x)^2}$.

For the first interior node

$$(1+\gamma)T_1^{\,l+1} - \gamma T_2^{\,l+1} = \gamma T_o^{\,l} + \gamma T_2^{\,l} + 2(1-\gamma)T_1^{\,l} + \gamma T_0^{\,l+1} \qquad (2.5)$$

For the last interior node

$$-\gamma T_{m-1}^{\,l+1} + 2(1+\gamma)T_m^{\,l+1} = \gamma T_{m-1}^{\,l} + \gamma T_{m+1}^{\,l} + 2(1-\gamma)T_m^{\,l} + \gamma T_{m+1}^{\,l+1} \qquad (2.6)$$

where $T_o^{\,l}$, $T_0^{\,l+1}$, $T_{m+1}^{\,l}$ and $T_{m+1}^{\,l+1}$ are prescribed as boundary conditions at top and bottom ends.

Consolidation of all the equations governing the nodes will yield a system of *m* equations, which in turn can be solved efficiently by *Gauss Seidel* method due to the amalgamated sparse matrix with most of the elements equal to zero. Therefore, the temperature rise of a dry soil medium exposed to high heat flux with adequate insulation, can be predicted using the Crank-Nicholson finite-difference method, provided the value of the effective thermal diffusivity of the soil medium can be reasonably estimated.

2.2.2 Convection Phenomena

Horton and Rogers (1945) and Lapwood (1948) were among the first to study the problem of a horizontal layer of porous medium heated from below. Their studies showed convection occurring within the porous medium when it was heated. Subsequently, other authors (Elder 1967, Katto and Masuoka 1967, Bau and Torrance 1982, Nield and Bejan 1999) followed by studying the onset of convection in porous medium in greater details and some (Shattuck et al 1997 and Howle 1997) employed specialized visualization techniques to observe images of the convection cells occurring in porous medium. In particular, Bau and Torrance (1982) developed analytical predictions for the onset of convection in the absence of boiling under steady-state conditions in a vertical cylinder filled with porous materials and heated from below. Bau and Torrance used linear stability analysis to calculate the theoretical critical Rayleigh number and found to be in good agreement with the experimental results.

The ensuing formulation based on linear stability analysis to predict the critical Rayleigh number analytically follows closely to that developed by Bau and Torrance (1982) as well as Nield and Bejan (1999). Notwithstanding that the analysis carried out by these authors is applicable for only *steady-state* conditions with *no boiling* which differs from our experimental conditions – transient state with boiling phenomenon, it provides qualitative insights into some useful characteristics such as the distinctive S-shaped temperature profile and the velocity profile that identify the occurrence of convection in porous medium. Furthermore, the governing equations

laid out in the following paragraph provide the foundation to build upon for the ongoing development of a predictive model describing the dynamics of convection and boiling phenomena in porous medium exposed to high heat flux.

Consider a vertical circular cylinder filled with porous medium with diameter D and height H with constant temperature applied at top and bottom, bounded at the sides and bottom by impermeable walls. Let z be the dimensionless height given by z^*/H where z^* is the dimensional height; v and w are the horizontal and vertical components of the velocity vector respectively. The schematic diagram is shown in Figure 4.

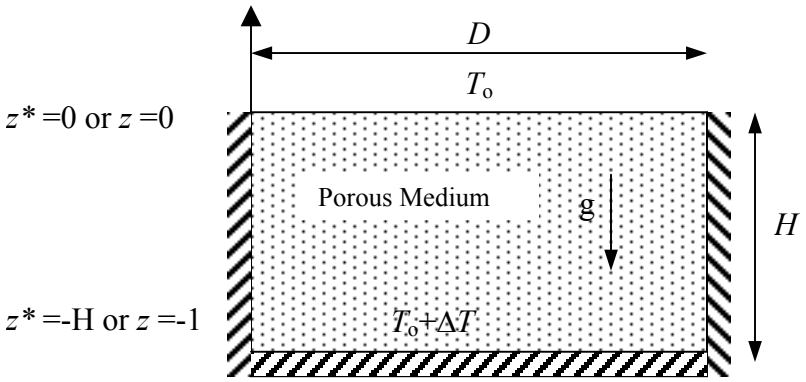

Figure 4. Schematic diagram of porous material heated from below

Assumptions:

(1) Local thermal equilibrium between fluid and soil particles (i.e. $T_s = T_f = T$);

(2) Negligible heating from viscous dissipation;

(3) Negligible radiative effect and pressure work term;

(4) No initial heat generation;

(5) Porous medium is isotropic and homogeneous;

(6) Negligible heat loss due to adiabatic side walls.

The four basic governing equations for the behavior of porous medium heated from below are given by:

Continuity equation: $$\nabla \bullet \boldsymbol{v} = 0 \tag{2.7}$$

Momentum equation: $$c_a \rho_o \frac{\partial \boldsymbol{v}}{\partial t} = -\nabla P - \frac{\mu}{\lambda}\boldsymbol{v} + \rho_f \boldsymbol{g} \tag{2.8}$$

Energy equation: $$(\rho c)_m \frac{\partial T}{\partial t} + (\rho c_p)_f \boldsymbol{v} \bullet \nabla T = k_e \nabla^2 T \tag{2.9}$$

Oberbeck-Boussinesq assumption: $$\rho_f = \rho_o [(1 - \beta(T - T_o))] \tag{2.10}$$

where c_a is the "acceleration coefficient tensor" which depends sensitively on the geometry of the porous medium; k_e is the effective thermal conductivity of the soil medium; $\mathbf{v}$ is the seepage velocity vector of fluid; $\boldsymbol{g}$ is the gravitational vector; μ is the fluid dynamic viscosity; λ is the permeability of the porous medium; T is the temperature; P is the pore water pressure; ρ is the density; ρ_o is the initial density; c_p is the specific heat capacity; $(\rho c)_m=(1-\phi)(\rho c)_s+ \phi(\rho c_p)_f$; ϕ is the porosity; β is the coefficient of thermal expansion; subscripts f and s represent fluid and soil particle respectively.

The steady state solutions to these equations (2.7) to (2.10) that satisfy the boundary conditions are given by:

$$\boldsymbol{v_b} = 0 \tag{2.11}$$

$$T_b = T_o - \Delta T\left(\frac{z^*}{H}\right) \tag{2.12}$$

$$P_b = P_o - \rho_o g\left[(z^* + H) + \frac{1}{2}\beta \Delta T\left(\frac{z^{*2}}{H} - H\right)\right] \tag{2.13}$$

Linear Stability Analysis

Substituting principal and perturbation forms of the dependent variables in the form $\boldsymbol{v} = \boldsymbol{v}_b + \boldsymbol{v}'$, $T = T_b + T'$, $P = P_b + P'$ where the perturbation quantities are considered to be small so that 2nd order small quantities can be neglected, and substituting Eqns (2.11) to (2.13) into Eqns (2.7) to (2.9) yields:

Continuity equation: $$\nabla \cdot \boldsymbol{v}' = 0 \tag{2.14}$$

Momentum equation: $$c_a \rho_o \frac{\partial \boldsymbol{v}'}{\partial t} = -\nabla P' - \frac{\mu}{\lambda}\boldsymbol{v}' - \beta \rho_o T' \boldsymbol{g} \tag{2.15}$$

Energy equation: $$(\rho c)_m \frac{\partial T'}{\partial t} - (\rho c_p)_f w' \frac{\Delta T}{H} = k_e \nabla^2 T' \tag{2.16}$$

A modified form of the momentum equation is obtained by operating twice with the curl. Only the *z*-direction momentum equation is retained for analysis. Furthermore, the perturbed flow is assumed to be steady resulting in the following non-dimensional form:

Continuity equation: $$\nabla \cdot \hat{\boldsymbol{v}} = 0 \tag{2.17}$$

Momentum equation: $$\nabla^2 \hat{w} = Ra^{1/2} \nabla_l{}^2 \hat{\theta} \tag{2.18}$$

Energy equation: $$\nabla^2 \hat{\theta} = -Ra^{1/2} \hat{w} \tag{2.19}$$

where

$$\hat{\theta} = \frac{T' - T_o}{\Delta T} + \frac{z^*}{H};\ \nabla_l{}^2 = \nabla^2 - \frac{\partial^2}{\partial z^2};\ Ra = \frac{g\lambda\beta\,\Delta T\, H}{\upsilon \alpha_m}(Rayleigh\ number);\ \hat{w} = \frac{Hw'}{Ra^{1/2}\alpha_m};$$
$$\hat{r} = \frac{r}{H}; \hat{t} = \frac{\alpha_m t}{\sigma H^2};\ \sigma = \frac{(\rho c)_m}{(\rho c_p)_f};\ \hat{P} = \frac{KP'}{\mu \alpha_m}; z = \frac{z^*}{H}; \alpha_m = \frac{k_e}{(\rho c_p)_f}.$$

Boundary conditions are then given by:

$\hat{v} = \dfrac{\partial \hat{\theta}}{\partial r} = 0$ at $r = \dfrac{D}{2H} = \gamma$ (aspect ratio);

$\hat{w} = \hat{\theta} = 0$ at $z = -1$;

$\dfrac{\partial \hat{w}}{\partial z} = \hat{\theta} = 0$ at $z = 0$

The governing equations and boundary conditions can be further reduced to:

$$\nabla^4 \hat{\theta} + Ra \nabla_l^{\,2} \hat{\theta} = 0 \qquad (2.20)$$

$\dfrac{\partial \hat{\theta}}{\partial r} = \nabla^2 \left(\dfrac{\partial \hat{\theta}}{\partial z} \right) = 0$ at $r = \gamma$ (aspect ratio);

$\hat{\theta} = \nabla^2 \hat{\theta} = 0$ at $z = -1$;

$\hat{\theta} = \nabla^2 \left(\dfrac{\partial \hat{\theta}}{\partial z} \right) = 0$ at $z = 0$

Eqn. (2.20) is solved using separation of variables to yield the following solution:

$$\hat{\theta} = Q(z) J_m (Z_{mp} \frac{r}{\gamma}) \cos(m \psi) \qquad (2.21)$$

where J_m = Bessel function of the first kind, m,p are integers, r and ψ are the radial and azimuthal co-ordinates respectively, $Q(z)$ is a function of z and Z_{mp} is the p^{th} zero of $\dfrac{\partial}{\partial r}\left(J_m (Z_{mp})\right)=0$.

The linear stability eigenvalue problem is expressed in terms of *Q(z)* after substituting Eqn. (2.21) into Eqn. (2.20):

$$(D^2 - k_{mp}^2)\, Q - k_{mp}^2 Ra\, Q = 0 \qquad (2.22)$$

where $D = d / dz$ and $k_{mp} = Z_{mp} / \gamma$

The transformed boundary conditions are given by:

$Q = D(D^2 - k_{mp}{}^2)Q = 0$ at $z = 0$

$Q = D(D^2 - k_{mp}{}^2)Q = 0$ at z =-1

In order to obtain the nontrivial solution to equation (2.22) with boundary conditions satisfied, there is a condition that must be satisfied which gives rise to the characteristic equation for *Ra*:

$$\xi \coth \xi + \eta \cot \eta = 0 \qquad (2.23)$$

where $\xi^2 = k_{mp}(Ra^{1/2} + k_{mp})$ and $\eta^2 = k_{mp}(Ra^{1/2} - k_{mp})$

The critical Rayleigh number at the onset of convection is then evaluated from the following inequalities:

$$(n-1)^2 \frac{\pi^2}{4k_{mp}{}^2} + k_{mp} < Ra^{1/2} < n^2 \frac{\pi^2}{k_{mp}} + k_{mp}$$

$\Rightarrow Ra_{cr} = \min_{m,n,p} Ra$ for a given aspect ratio γ

For minimum Ra_{cr} value, let n = 1 and (m, p) refers to the preferred convection modes. The aspect ratio for the experimental configuration $\gamma = D/2H$ =0.2 where *D* is the diameter of the soil column and *H* is the differential heated soil column height. It should be noted that in this investigation, the soil column height definition is limited to the portion of the differentially heated soil column where significant temperature gradients exist. According to Bau and Torrance, the computed aspect ratio yields a preferred mode of convection (m = 1, p = 1) as depicted in Figure 5.

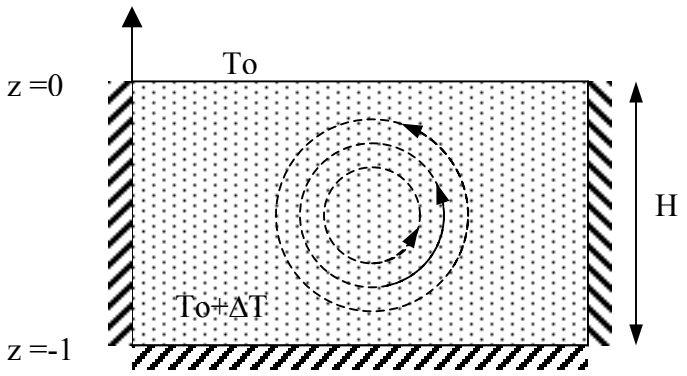

Figure 5. Schematic description of convective mode (1,1) in porous medium heated from below.

Subsequently, Eqn. (2.22) can be solved to yield a solution for *Q(z)* and the result is given:

$$Q(z) = \frac{\sin \eta(z+1)}{\sin \eta} + \frac{\sinh \xi(z+1)}{\sinh \xi} \tag{2.24}$$

Combining Eqns (2.18), (2.19), (2.21) and (2.24), the vertical component of the velocity (*w*) is determined to be:

$$\hat{w} = W(z) J_m(\kappa_{mp} r)\cos(m\psi) \tag{2.25}$$

$$W(z) = \frac{\kappa_{mp}}{Ra^{1/2}}\left(\frac{\sin \eta(z+1)}{\sin \eta} + \frac{\sinh \xi(z+1)}{\sinh \xi}\right) \tag{2.26}$$

where $\kappa_{mp} = Z_{mp}/\gamma$; Z_{mp} is the p^{th} zero of $\frac{\partial}{\partial r} J_m(Z_{mp}) = 0$; J_m is the Bessel function of the first kind; $\xi^2 = \kappa_{mp}(Ra^{1/2} + \kappa_{mp})$; $\eta^2 = \kappa_{mp}(Ra^{1/2} - \kappa_{mp})$; r and ψ are the radial and azimuthal co-ordinates respectively.

Nield (1968) developed different values of critical Rayleigh number Ra_{cr} for different boundary conditions for an infinite horizontal porous medium heated from below as shown in Table 2. Based on Table 2, $(Ra_{cr})_{theory}$= 27.1 at the onset of convection for the specific boundary conditions applicable to our experiment and neglecting the effects of boiling.

Table 2. Values of the critical Rayleigh number Ra_{cr} and the corresponding critical wavenumber α_c for the various boundary conditions (Nield 1968). Subscripts *l* and *u* represent lower and upper bounds respectively.

IMP: Impermeable(K= ∞) CON: Conducting or Constant Temp (L = ∞)			FREE: Free (K=0) INS : Insulating or Constant Heat Flux (L=0)		
K_l	K_u	L_l	L_u	Ra_{cr}	α_c
IMP	IMP	CON	CON	39.48 or $4\pi^2$	3.14 or π
IMP	IMP	CON	INS	27.1	2.33
IMP	IMP	INS	INS	12	0
IMP	**FREE**	**CON**	**CON**	**27.1**	**2.33**
IMP	FREE	INS	CON	17.65	1.75
IMP	FREE	CON	INS	9.87 or π^2	1.57 or π/2
IMP	FREE	INS	INS	3	0
FREE	FREE	CON	CON	12	0
FREE	FREE	CON	INS	3	0
FREE	FREE	INS	INS	0	0

The following equations demonstrate how the various permutations of K_l, K_u , L_l, L_u relate to the different types of boundary conditions imposed.

At z = -1 (bottom), the applicable kinetic and thermal boundary conditions are expressed as $H\frac{\partial w}{\partial z} - K_l w = 0$ and $H\frac{\partial \theta}{\partial z} - L_l \theta = 0$ respectively.

As $w \to 0, K_l = \frac{\frac{\partial w}{\partial z} H}{w} \to \infty$ (impermeable)

As $\theta \to 0, L_l = \frac{\frac{\partial \theta}{\partial z} H}{\theta} \to \infty$ (constant temperature boundary)

At z = 0 (top), the applicable kinetic and thermal boundary conditions are expressed as $H\frac{\partial w}{\partial z} + K_u w = 0$ and $H\frac{\partial \theta}{\partial z} + L_u \theta = 0$ respectively.

For soil medium bounded at the top by the standing fluid identical with the saturating medium, $\frac{\partial w}{\partial z} = 0 \Rightarrow \frac{-\frac{\partial w}{\partial z}H}{w} = K_u \to 0$

Similarly, $L_u = \frac{-\frac{\partial \theta}{\partial z}H}{\theta} \to 0$ since $\frac{\partial \theta}{\partial z}$ is likely to be small or equal to 0.

Knowing that the preferred convection mode is (1, 1) and aspect ratio $\gamma \approx 0.2$, appropriate values of the properties of water and sand based on time-averaged values (e.g. $\Delta T \approx 50^{o}$C) can be substituted into Eqn. (2.25) to generate the representative velocity profile at z = -0.5 under steady-state conditions which is described in Figure 6 below.

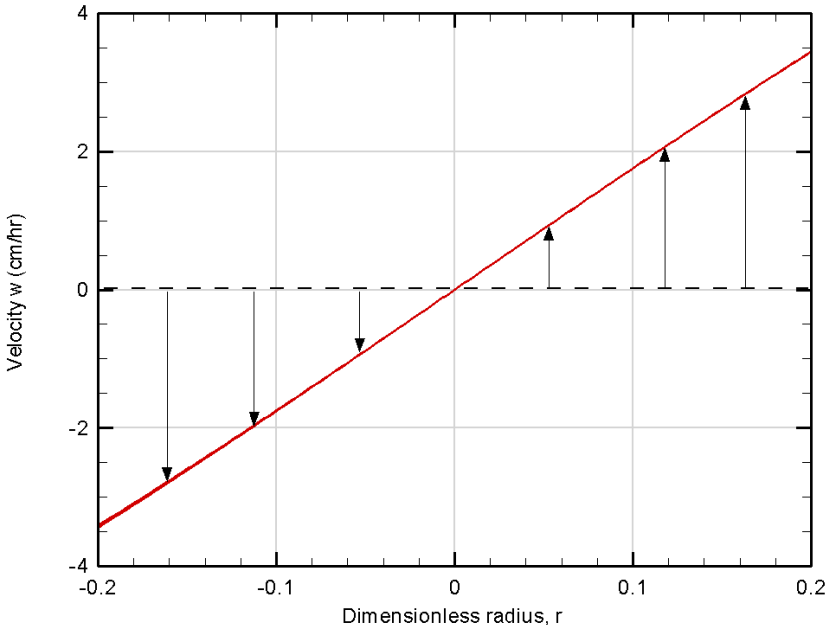

Figure 6. Representative analytical velocity profile for convective mode (1,1) at z = -0.5.

Similarly, the temperature profile is determined to be:

$$\frac{T-T_o}{T_l-T_o}=\frac{A}{Ra}\theta(z)J_m(\kappa_{mp}r)\cos(m\psi)+\frac{A^2}{Ra}\int_0^z W\theta dz-Nuz \qquad (2.27)$$

where $\dfrac{Nu-1}{1-\dfrac{Ra_{cr}}{Ra}}=\left(\dfrac{\left(\int_{-1}^{0}FW\,dz\right)^2}{\int_{-1}^{0}F^2W^2\,dz-\left(\int_{-1}^{0}FW\,dz\right)^2}\right)$, $F=(D^2-\kappa_{mp}{}^2)W$,

$A^2=-\kappa_{mp}{}^2(Ra-Ra_{cr})\dfrac{\int_{-1}^{0}FW\,dz}{\int_{-1}^{0}F^2W^2\,dz-\left(\int_{-1}^{0}FW\,dz\right)^2}$, $D=\dfrac{d}{dz}$ and

$$Q(z)=\frac{\sin\eta(z+1)}{\sin\eta}-\frac{\sinh\xi(z+1)}{\sinh\xi}$$

Since the temperature profile for our experimental configuration is transient and changes continuously with time, a representative temperature profile using Eqn. (2.27) based on time-averaged values (e.g. $\Delta T \approx 50^{o}$C) is drawn analytically in Figure 7 to illuminate the expected behavior of the convection phenomenon within the soil media at one particular moment.

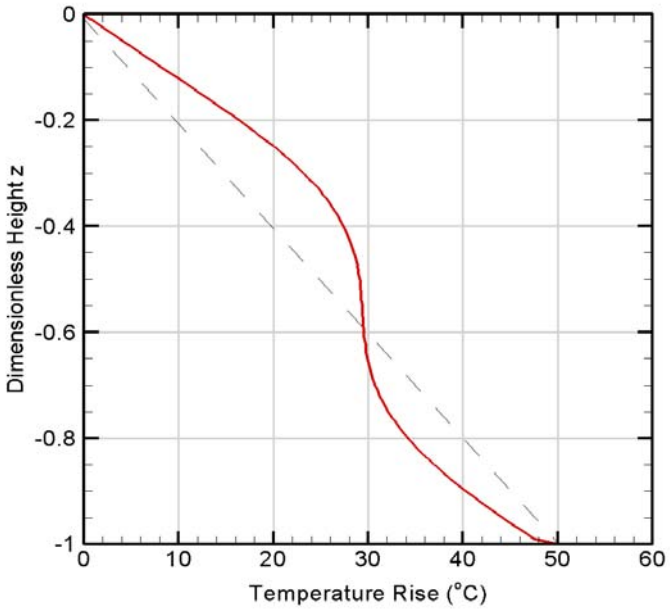

Figure 7. Characteristic S-shaped temperature profile indicating convection motion in mode (1, 1).

It can be observed that the onset of convective mode causes the temperature profile to form a distinctive S-shape, decreasing asymmetrically along the linear temperature profile (conduction-dominant mode). At the onset of convection, the ascending warm water causes the temperature at the top to be higher and the descending cold water causes the temperature to be lower compared to that of pure conduction. It is further noted that the temperature profile is not symmetric about the mid plane (i.e. z = -0.5) because of the different boundary conditions at the top and bottom faces.

2.2.3 Boiling Phenomena

Bau and Torrance (1982) observed the formation of a two-layer system under steady-state conditions at the onset of boiling in a horizontal water-saturated porous medium heated from below. The two-layer system has an almost isothermal, two-phase zone underlying the liquid layer as shown in Figure 8. Their experiment also revealed that the two-phase region is essentially isothermal at the saturation temperature and may be liquid or vapor-dominated.

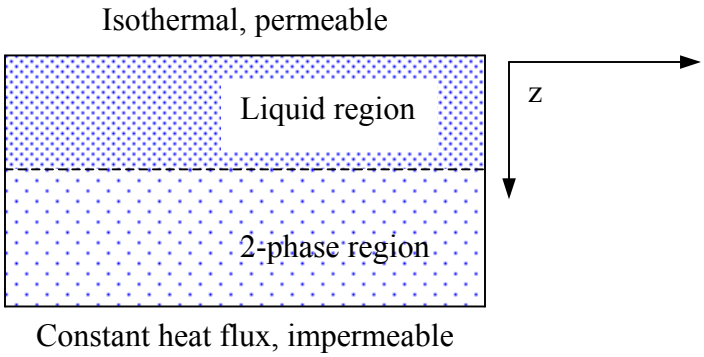

Figure 8. Schematic diagram of a two-layers system at onset of boiling for a porous medium heated from below.

Heat is transmitted through the two-phase region by the counter-percolating flow of liquid and vapor driven by buoyancy in which the liquid vaporizes at the lower heated boundary of the two-phase region and the vapor condenses at the interface between the two-phase and liquid regions. Heat transfer in the liquid region may take place either by conduction or convection. Ramesh and Torrance (1990) found that the two important parameters that characterize the boiling phenomenon in a water-saturated porous medium heated from below are namely Rayleigh number, *Ra,* which describes the buoyancy effects and the dimensionless heat flux at the bottom boundary, $Q_b = q_b H/k_e(T_{sat}-T_o)$ which determines the height of the two-phase region.

Using the approach outlined by Ramesh and Torrance, and analogous dimensionless transformation described in §2.2.2, the governing equations in the liquid and two-phase regions in dimensionless forms are expressed as:

For the liquid region:

Continuity equation: $$\nabla \bullet \hat{\boldsymbol{v}}_l = 0 \tag{2.28}$$

Momentum equation: $$\hat{\boldsymbol{v}}_l = -\nabla \hat{P} - Ra\, \hat{T}\, \boldsymbol{e}_z \tag{2.29}$$

Energy equation: $$\eta_1 \frac{\partial \hat{T}}{\partial t} + \hat{\boldsymbol{v}}_l \bullet \nabla \hat{T} = \nabla^2 \hat{T} \tag{2.30}$$

For the two-phase region:

Continuity equation: $$\eta_2 \frac{\partial S}{\partial t} + \nabla \bullet (\hat{\boldsymbol{v}}_l + \overline{\rho}_v \hat{\boldsymbol{v}}_v) = 0 \tag{2.31}$$

Momentum equation: $$\hat{\boldsymbol{v}}_l = -k_{rl}(\nabla \hat{P} + Ra\, \boldsymbol{e}_z) \tag{2.32}$$

$$\hat{\boldsymbol{v}}_v = -k_{rl}\overline{\mu}_l(\nabla \hat{P} + Ra_{2\phi}\, \boldsymbol{e}_z) \tag{2.33}$$

Energy equation: $$\phi \overline{\rho}_v \zeta \frac{\partial (1-S)}{\partial t} + \nabla \bullet (\overline{\rho}_v \zeta\, \hat{\boldsymbol{v}}_v) = 0 \tag{2.34}$$

where $$\eta_1 = \frac{(\rho c)_m}{(\rho c_p)_l}; Ra_{2\phi} = \frac{(1-\overline{\rho}_v)Ra}{\beta_l (T_{sat} - T_o)}; \overline{\rho}_v = \frac{\rho_v}{\rho_l}; \overline{\mu}_l = \frac{\mu_l}{\mu_v}; \zeta = \frac{h_{fg}}{c_{pl}(T_{sat} - T_o)};$$

$\eta_2 = \phi(1 - \overline{\rho}_v)$; $\hat{\boldsymbol{v}}$ is the velocity vector; k_{rl} and k_{rv} are relative the permeability for the liquid and vapor phases respectively which are typically functions of S; ϕ is the porosity; $\hat{T}$ is the temperature; $\hat{P}$ is the pressure; S is the degree of liquid saturation in the two-phase region where S = 0 connotes 100% vapor phase; subscripts l and v

represent liquid and vapor phase respectively; $\boldsymbol{e}_z$ is a unit vector in z which is assumed positive in the direction of gravity vector.

It can be deduced that the two Rayleigh numbers Ra and $Ra_{2\phi}$, in the liquid and two-phase regions respectively, are related and their relationship can be expressed as:

$$\psi = \frac{Ra}{Ra_{2\phi}} = \frac{\beta_l (T_{sat} - T_o)}{1 - \overline{\rho}_v}$$

Note that ψ is a parameter that depends on the ratio of the density between the phases in the two-phase region and the liquid thermal expansion coefficient, provided ΔT is assumed constant.

Assuming linear relative permeabilities i.e. $k_{rl} = S$ and $k_{r\,v} = 1\text{-}S$, and applying linear stability analysis with the applicable boundary conditions, Eqns (2.28) to (2.34) are solved numerically by Ramesh and Torrance to yield the steady-state solutions. The solutions are plotted in Figures 9 and 10. Figure 9 shows that the two-phase region can either be vapor-dominated or liquid-dominated for a given magnitude of heat flux and there is a maximum heat flux beyond which the two-phase region does not exist i.e. the complete vaporization of the liquid phase.

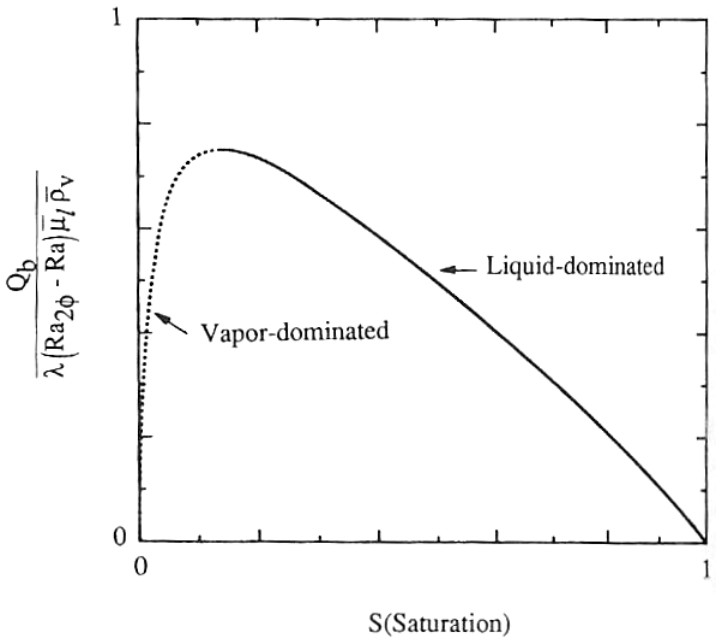

Figure 9. Plot of heat flux against saturation in a two-phase system (Ramesh and Torrance, 1990).

Boiling in a porous medium heated from below produces a unique system where there is a two-phase zone underlying a single-phase liquid zone. This phenomenon presents two mechanisms for instability i.e. a convective instability driven by buoyancy within the liquid zone and a gravitational instability due to the denser liquid zone overlying the lighter two-phase zone. Schubert and Straus (1980) studied this problem and found that the stability of such system is provided by phase change processes at the interface in which the distortion of interface occurs.

The curve ABE in Figure 10 indicates the onset of boiling above which the liquid-dominated two-phase region will occur. It can be inferred that there are four different possible regimes with distinct combinations of convection, conductive and boiling

modes that could occur in a porous media heated from below depending on the Rayleigh number and heat flux.

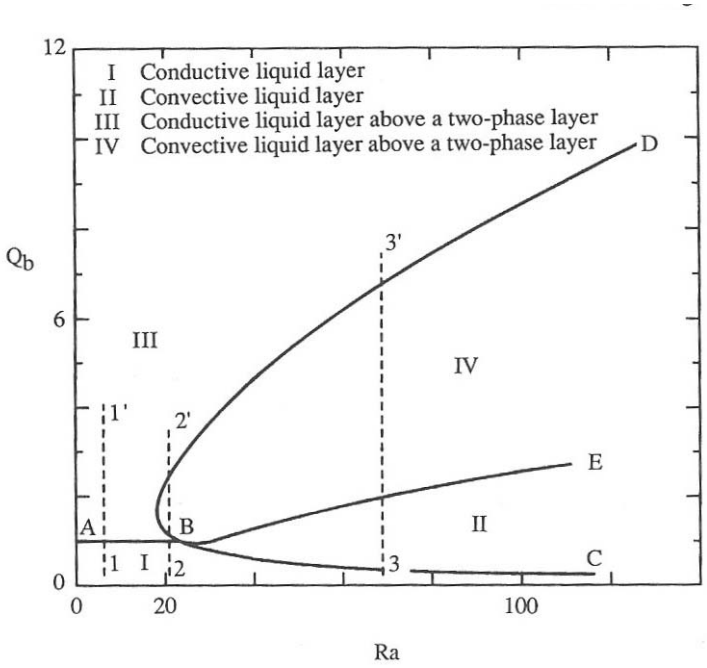

Figure 10. Map of conductive and convective solutions in (Ra, Q_b) space for liquid-dominated two-phase system for wave number =π (Ramesh and Torrance 1990).

2.2.4 Multi-Phase Flow

In a porous medium where the void space is occupied by two or more miscible fluids such as steam and water (two-phase), the heat and mass flow analysis of this multi-component mixture will be more complex, invoking the use of the concept of relative permeabilities in combination of Darcy's Law. From Nield and Bejan (1999), the overall volume-averaged governing equations for a multi-phase flow in a porous media are given:

Assumptions:

(1) Local thermal equilibrium;

(2) Negligible viscous dissipation;

(3) Negligible radiative effects;

(4) No initial heat generation;

(5) Negligible pressure work term; and

(6) Negligible capillary pressure.

Continuity equation:

$$\frac{\partial}{\partial t}\left[\phi S_l \rho_l + \phi S_v \rho_v + (1-\phi)\rho_s\right] + \nabla.(\rho_l \boldsymbol{v}_l + \rho_v \boldsymbol{v}_v + \rho_s \boldsymbol{v}_s) = 0 \qquad (2.35)$$

Momentum equation:

$$\boldsymbol{v}_l - \frac{\varepsilon_l}{\varepsilon_s}\boldsymbol{v}_s = -\frac{k_{rl}\lambda}{\mu_l}\left(\nabla P - \rho_l \boldsymbol{g}\right) \qquad (2.36)$$

$$\boldsymbol{v}_v - \frac{\varepsilon_v}{\varepsilon_s}\boldsymbol{v}_s = -\frac{k_{rv}\lambda}{\mu_v}\left(\nabla P - \rho_v \boldsymbol{g}\right) \qquad (2.37)$$

Energy equation:

$$\begin{aligned}&\frac{\partial}{\partial t}\left[\phi S_l \rho_l h_l + \phi S_v \rho_v h_v + (1-\phi)\rho_s h_s\right] + \nabla.(\rho_l h_l \boldsymbol{v}_l + \rho_v h_v \boldsymbol{v}_v + \rho_s h_s \boldsymbol{v}_s) \\ &- \nabla.(k\nabla T) - \left[\frac{\partial P}{\partial t} + (\boldsymbol{v}_l + \boldsymbol{v}_v + \boldsymbol{v}_s).\nabla P\right] = 0\end{aligned} \qquad (2.38)$$

where $\varepsilon_i = V_i / V_{tot}$; V is the volume; subscripts $\boldsymbol{v}$ is the velocity vector; *l, v* and *s* represent the liquid, vapor and solid phases respectively; *S* is the degree of saturation; *h* is the enthalpy; k_{rl} and k_{rv} - relative permeability for the liquid and vapor phases respectively; the other terms have been mentioned previously.

One of the complications in modeling multi-phase flow in porous medium is the difficulty of predicting the variation of the relative permeabilities with different degrees of saturation, although a simple linear relationship has been proposed.

2.3 Response of Soil At Extreme Elevated Temperature

Many authors (Campanella and Mitchell 1968, Plum and Esrig 1968, Houston et al. 1985, Houston and Lin 1987, Sherif and Burrous 1969) have investigated the response of saturated soils to elevated temperature with no temperature gradient across the soil specimens. It is found that generally, temperatures increase for saturated soils under drained condition at constant effective stress results in permanent volumetric shrinkage with a lower void ratio, increase in compressive stress and shear strength of the soil structure after cooling of the specimens. For temperature rise at undrained condition, excess pore water pressure could build up significantly due to the differential expansion of the water and soil particles, and physico-chemical effects.

2.3.1 Definitions of Shear Strength and Effective Normal Stress of Soil

In order to assess the effects of temperature on the mechanical properties of soil, it is important to understand the fundamental equations governing the pore pressure, shear strength, void ratio and normal effective stress. The shear strength τ of saturated cohesiveless soil is approximated by (Mitchell 1993):

$$\tau = \sigma_{eff} \tan \phi_f \qquad (2.39)$$

where σ_{eff} is the effective normal stress and ϕ_f is the friction angle. Typically, ϕ_f varies from 30^o to 50^o for quartz sand.

The effective normal stress is further described as follows:

$$\sigma_{eff} = \sigma - \upsilon_w \tag{2.40}$$

where σ is the normal stress and υ_w is the pore water pressure. It has been found that generally, the lower the void ratio *e* (defined as the ratio of the volume of void to the volume occupied by solid particles), the higher the shear strength of the soil medium (Mitchell 1993, Terzaghi 1925) although it is not fully resolved whether the relationship is linear.

2.3.2 Mechanisms of Consolidation At Elevated Temperature

In their paper, Campanella and Mitchell (1968) postulated that two effects occur when the temperature of a soil specimen is increased. A rapid temperature rise, even under drained conditions, will cause the pore water pressure to increase steeply due to the greater volumetric expansion of the water relative to the solid particles. The lower the permeability of the soil, the longer the time for the pore water pressure to be dissipated. As pore pressure dissipates, the liquid will be driven out of the soil medium due to the pore water pressure gradient and densification occurs i.e. the phenomenon of primary consolidation. It should be noted that for our experiments, the expansion associated with the phase change at saturation temperature could amplify the buildup of the pore water pressure, thereby further contributing to the primary consolidation effect.

The second effect relates to the decrease in the strength of the soil structure with increasing temperature. The rise in pore pressure will lead to a drop in the effective normal stress which in turn causes a reduction in the shear strength of the soil medium. Subsequently, there is a partial collapse and deformation of structure of the soil medium i.e. secondary compression resulting in a lower void ratio until a sufficient number of inter-particle bonds are formed to withstand the stress at the higher temperature. This secondary compression depends on the properties of the soil structure and is independent of the pore water pressure. Consequently, the soil structure is strengthened after densification in response to temperature elevation. Houston et al. (1985) also observed that the densification of soil increases with increasing temperature rise.

Campanella and Mitchell further observed that that there is an overall irreversible volume reduction in the soil specimen after an initial heat-cool cycle where water re-absorbed into the specimen during temperature decrease was less than the amount drained out during temperature increase. This is because the densification caused by the secondary compression effect is irreversible even when the temperature is decreased upon cooling. In addition, the secondary compression effect is negligible for subsequent heat-cool cycles since the soil structure has been previously strengthened, provided that the initial temperature increase is not exceeded.

According to Mitchell (1993), the mathematical relationship between void ratio e and the effective normal stress σ_{eff} is described as follows:

$$e = f(\sigma_{eff}, t) \Rightarrow \frac{de}{dt} = \left(\frac{\partial e}{\partial \sigma_{eff}}\right)_t \frac{d\sigma_{eff}}{dt} + \left(\frac{\partial e}{\partial t}\right)_{\sigma_{eff}} \tag{2.41}$$

The first and second terms are commonly referred as the primary consolidation and secondary compression respectively. The primary consolidation depends on the Darcy's law which, in turn determines the rate at which the pore water drains under the pressure gradient whilst the secondary compression is affected by how fast the soil structure deforms under a given normal stress.

2.3.3 Pore Water Pressure

The upshot of a literature survey (e.g. Green 1984, Houston and Lin 1987, Lin 1985, Mitchell 1993) appears that it is difficult to model or predict the pore water pressure increase accurately in saturated soils subjected to elevated temperature based on theoretical principles alone. Campanella and Mitchell (1968) derived a simplified expression for the increase in pore water pressure, ΔP due to increase in temperature ΔT for fully saturated soils under undrained conditions as follows:

$$\Delta P = \frac{\phi \, \Delta T \, (\beta_s - \beta_w) + \beta_{st} \Delta T}{m_v} \tag{2.42}$$

in which β_s and β_w refer to the thermal coefficient of volumetric expansion for soil particles and water respectively; β_{st} is the physico-chemical coefficient of structural volume change caused by ΔT; m_v is the compressibility of the soil structure, and ϕ is the porosity.

Therefore, it can be deduced that the key factors affecting the pore water pressure are namely (1) change in temperature, (2) the porosity of the soil matrix, (3) the differential expansion between the soil particles and water, (4) the volume change in soil structure due to physico-chemical effects as a result of elevated temperature and (5) compressibility of the soil structure. Based on Eqn. (2.42), the lower the compressibility of the soil structure, the greater the pore water pressure for a given ΔT under undrained condition.

Campanella and Mitchell (1968) further suggested using a pore pressure parameter F to estimate the temperature-induced pore water pressure for different soils under different test conditions. The pore pressure parameter F is defined as the change in the pore pressure per unit change in temperature per unit effective stress and is expressed as

$$F = \frac{\frac{\Delta P}{\Delta T}}{\sigma_{eff}} \qquad (2.43)$$

They compared the measured pore water pressure results from triaxial tests conducted by several authors (Campanella and Mitchell 1968, Henkel and Sowa 1963, and Ladd 1961) and found that the parameter F remained relatively constant for a wide range of

the effective stresses for a particular soil type. Moreover, they noticed that the higher the effective stress, the greater the pore water pressure built up in the soil medium. Table 3 shows the different values of F under different test conditions for different soil types, extracted from Campanella and Mitchell (1968).

Table 3. Temperature-induced pore water pressure for different soil type

Soil Type	σ_{eff} (kg/cm^2)	ΔP (kg/cm^2)	ΔT (^{o}F)	$F = \frac{\frac{\Delta P}{\Delta T}}{\sigma_{eff}}$ $(^o F)^{-1}$
Illite	2.0	0.58	70 – 110	0.0073
Weald Clay	7.1	0.51	70 – 110	0.0083
Kaolinite	2.0	0.78	70 – 110	0.0097
Vicksburg Buckshot Clay	1.0-6.5	0.28-1.9	68 – 96.8	0.0097 – 0.0101
Saturated Porous Stone	2.5-5.8	1.9-5.2	41.5 – 59	0.044 – 0.051

2.3.4 Stress-Strain Changes At Elevated Temperature

Houston et al. (1985) investigated the stress-strain behavior of soils subjected to elevated temperature up to 200^{o}C. The specimens were subjected to standard triaxial compressive strength tests at the end of the thermally-induced consolidation. It has been found that the peak shear strength of the specimens and stiffness of the soils increase with increasing temperature under drained conditions, which in turn is caused by the volumetric strain undergone during the thermal consolidation mechanism described in §2.3.2. Contrary to the behavior of lower temperature specimens, the strain behavior of the soils at high temperature (i.e. 200^{o}C) is brittle, showing very high peak strength at small axial strain, follows by significant strain softening resulting in a lower residual strength, typical of the characteristics of an

over-consolidated clay. The strain softening behavior of soils at high temperature is attributed to the lower void ratio at higher temperature, which makes the soils more susceptible to shearing along thin planes. Thus, the stress-strain behavior of soils is changed dramatically when exposed to high temperature. The experiments conducted by Laguros (1969) indicated similar progressive increase in peak stress strength with increasing temperature for 4 different clay soils.

2.4. Stability of Tunnel Lining

The deformation of the tunnel lining is not governed by its stiffness and bending strength, but rather it is controlled by the properties of the surrounding soil structure. In most cases, the tunnel lining behaves like an elastic ring whose ability to conform to the imposed deformation, as a result of a load acting on the lining, is instrumental to its stability. Figure 11 shows the various behaviors of the flexible lining ring under different loading and boundary conditions. It demonstrates that a confining boundary condition which hinges on the positive soil-lining interaction, results in smaller lining deformation compared to those cases subject to unconfined condition. Consequently, it can be inferred that the stability design of a tunnel lining is not based on rigorous structural analysis but depends critically on the soil-structure interaction instead. Furthermore, the Tunneling Engineering Handbook (1996) highlighted the most serious structural problems to be considered for the design of the lining are related to the absence of support induced by the presence of voids.

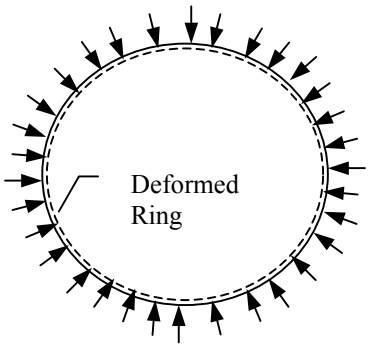

(a) Unconfined ring, uniform load

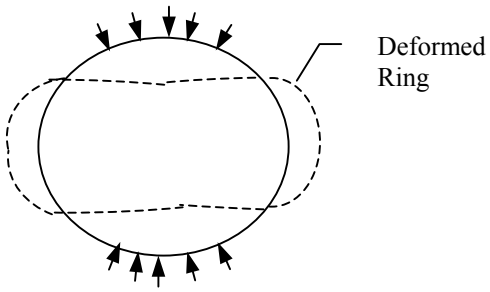

(b) Unconfined ring, concentrated load

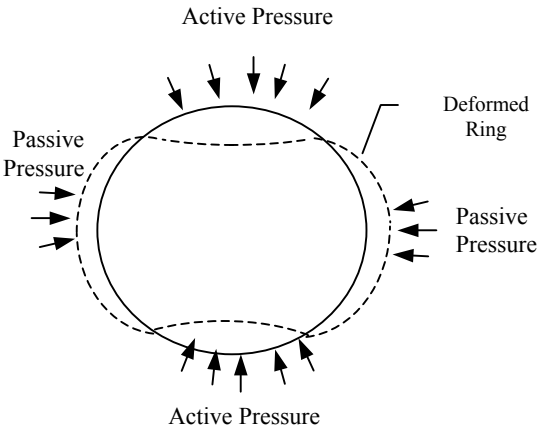

(c) Partially confined ring, concentrated load

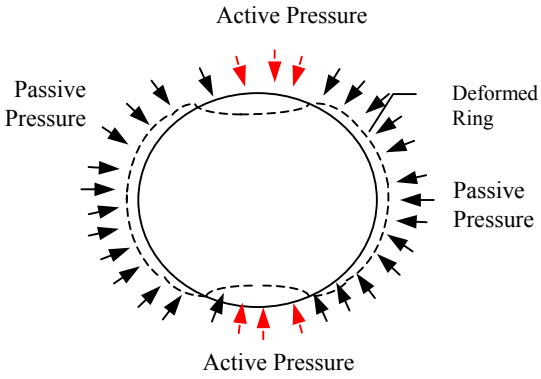

(d) Fully confined ring, concentrated load

Figure 11. Various Behaviors of Flexible Lining Ring Under Different Loading and Boundary Conditions.

CHAPTER 3: EXPERIMENTAL METHODOLOGIES

In this chapter, information on the different soil types, saturation conditions, type of measurements performed in our experiments as well as the soil thermal properties are presented. The relevance and concepts of the key parameters that characterize soil dynamics when heated are also elucidated. This is then followed by the description of the experimental procedures and setup.

3. 1 Methodologies

3.1.1 Test Matrix

In order to examine the geotechnical response of different soil types to intense heat, experiments were conducted for three different soil types involving coarse sand, fine sand, and silt. In addition, three different soil conditions -- dry, fully saturated, and partially saturated were studied for the soils. These conditions are intended to represent the range of realistic soil conditions occurring naturally. In all, 30 tests were conducted, and of those, 14 provided insight into soil response. Table 4 provides a summary of the different soil types, soil conditions and the myriad of the measurements performed in the experiments.

Table 4. Test matrix showing different test conditions and measurements.

S/N	Type of medium tested		Type of measurements
1a	Coarse Quartz	Dry soil	Pore pressure at different elevations
			Temperature profile at different elevations
			Density
			Heat Flux
b		Saturated soil	Pore pressure at different elevations
			Temperature profile at different elevations
			Density
			Boiling mechanism –bubbles
			Heat Flux
			Soil migration
c		Partially saturated soil	Pore pressure at different elevations
			Temperature profile at different elevations
			Density
			Residual moisture content at different elevations (after heating)
			Boiling mechanism –bubbles
			Heat flux
			Estimated residual moisture content before heating
2a	Fine Quartz	Dry soil	Pore pressure at different elevations
			Temperature profile at different elevations
			Density
			Heat Flux
b		Saturated soil	Pore pressure at different elevations
			Temperature profile at different elevations
			Density
			Boiling mechanism –bubbles
			Soil migration
			Heat Flux
c		Partially saturated soil	Pore pressure at different elevations
			Temperature profile at different elevations
			Density
			Residual moisture content at different elevations (after heating)
			Boiling mechanism –bubbles
			Heat Flux
			Soil migration
3	Silt	Saturated	Pore pressure at different elevations
			Temp profile at different elevations
			Residual moisture content at different elevations (after heating)
			Density
			Soil migration
			Heat Flux

3.1.2 Soil Properties

Since the dependence of fire-induced behavior of soils is inevitably linked to its thermal properties, it is valuable to determine the thermal transport properties of soils. In his report, Sundberg (1988) described an extensive background of thermal properties of soils and rocks. The thermal properties of a material depend on a number of factors, some of which can be time-dependent. The thermal conductivity of crystalline rock is mainly influenced by the following factors:

- mineral composition;
- temperature;
- isotropy / anisotropy characteristics;
- the absence or presence of, and properties of, fluid and gas in micro fissures.

Quartz is a common component of soils, and is the principal component of soils used in this research. It has a typical thermal conductivity of 8 W/m-K which is several times higher than that of other common rock forming minerals. Three different quartz soils were tested namely fine sand, coarse sand, and silt. All soils are commercially produced and were purchased from the U.S. Silica Company in Berkeley Springs, WV. The fine sand was grade F-62, the coarse sand was grade #3 Q-ROK, and the silt was grade Sil-Co-Sil 53. Each soil was free of any organic compounds. The benefit of using commercial grade quartz is to achieve relatively uniform grain size and identical mineral constant, resulting in isotropic thermal soil properties. Table 5 shows the summary of the overall thermal properties of the different soil type used.

Table 5. Properties for the different soil type.

Soil Type	Average grain size (μm)	Permeability, λ (m^2)	Average Porosity, ϕ (%)	Effective thermal conductivity, k_{eff} (W/m.K)
Coarse Sand	1000	2.3×10^{-9}	48%	2.2
Fine Sand	300	7.2×10^{-11}	38%	2.8
Silt	150	1×10^{-11}	33%	1.2 to 2.4*

*Sundberg(1988)

Sundberg (1988) reported that simple geometric mean method developed by Johansen (1975) has often been used as an accurate approximation of the effective thermal conductivity of fully saturated soils notwithstanding its lack of a theoretical basis i.e.

$k_{eff} = \prod_{i=1}^{n} k_i^{v_i}$ where v_i is the volume fraction and k_i is the constituent thermal conductivity. Therefore, effective thermal conductivity values for *fully saturated* coarse and fine quartz sands can be estimated using the geometric mean as follows:-

Substituting k_{quartz}= 7 W/m.K and k_{water}= 0.65 W/m.K at $T_{average}$=330K,

$$k_{eff,coarse} = \prod_{i=1}^{n} k_i^{v_i} = (7)^{0.5} \times (0.65)^{0.5} = 2.2 \quad \text{W/m.K}$$

$$k_{eff,fine} = \prod_{i=1}^{n} k_i^{v_i} = (7)^{0.6} \times (0.65)^{0.4} = 2.8 \quad \text{W/m.K}$$

It is noteworthy that the estimated values determined using the geometric mean method for *fully saturated* coarse and fine quartz sands lie within the minimum and maximum bounds established based on heat conduction in the porous medium occurring in series and parallel respectively (Nield and Bejan 1999, Highway Research Board 1969). Refer to Appendix A for details regarding the calculations of the bounds.

In addition, the effective permeability of the soils can be estimated using Kozeny-Carmen formula as shown:

$$\lambda_{fine} = \frac{d^2}{180} \times \frac{\phi^3}{(1-\phi)^2} = \frac{(0.3\times10^{-3})^2}{180} \times \frac{0.38^3}{(1-0.38)^2} = 7.2\times10^{-11}\,\mathrm{m}^2$$

$$\lambda_{coarse} = \frac{d^2}{180} \times \frac{\phi^3}{(1-\phi)^2} = \frac{(1.0\times10^{-3})^2}{180} \times \frac{0.48^3}{(1-0.48)^2} = 2.3\times10^{-9}\,\mathrm{m}^2$$

$$\lambda_{silt} = \frac{d^2}{180} \times \frac{\phi^3}{(1-\phi)^2} = \frac{(0.15\times10^{-3})^2}{180} \times \frac{(0.33)^3}{(1-0.33)^2} = 1\times10^{-11}\,\mathrm{m}^2$$

where d and ϕ are average grain diameter and porosity respectively.

3.1.3 Experimental Procedures

The detailed experimental procedures for the preparation of the soil column and setting up of the test apparatus are spelled out in Appendix B and will not be mentioned here. Once the testing apparatus was set up properly and filled with the course sand/fine sand/silt, the soil column was heated from the bottom until the temperature at the top reached an equilibrium value. The duration of each experiment typically varied between 2 to 8 hours. Most experiments were run as a suite of three (refer to Figure 12 for illustration) using the same sand sample in sequence namely *dry, fully saturated and partially saturated*. Tests began with a dry sand experiment. After completion of the dry sand experiment and the temperature returned to ambient, water was added to the soil slowly through a valve attached near to the base of the test apparatus until the water level reached the top of the soil column. Another test was then run on the fully saturated specimen. After the completion of the fully saturated sand experiment, water was drained leaving a moist specimen, and the same

experiment was run on the partially saturated sand. The draining process usually took more than 4 hours till there was negligible outflow of water from the soil column, leaving a moist specimen.

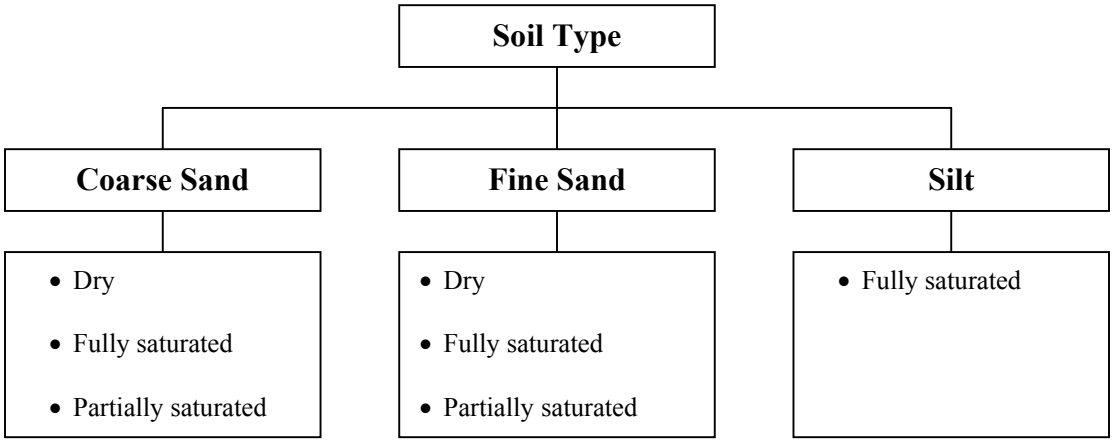

Figure 12. Matrix of test conditions.

The tests involving silt were prepared and performed in a different manner than the sand tests principally because of difficulties in placing a uniform saturated specimen of silt. Silt was first mixed with water in a bowl and stirred well to achieve a fully uniform saturation. The moisture content of the silt was set to approximately 33% mass of volume. After thorough mixing, the fully saturated silt was placed carefully into the testing tube up to the elevation of the 10^{th} thermocouple (about 254 mm from the bottom). The column between the 10^{th} and 16^{th} thermocouples was filled with fully saturated fine sand because of the onerous task to prepare a full 1.2 m high silt column. The instrumentation and other experimental procedures remained unchanged.

The temperature, the pressure, and the height of the water within the test apparatus (for fully saturated soil) were measured continuously and later analyzed. After the experiments, soil specimens were collected from different elevations during the dissection in order to determine the residual water content of the soil. The "ASTM Standard Test Method for Laboratory Determination of Water (Moisture) Content of Soil and Rock by Mass" (Designation: D 2216–98) was used to determine the residual water content of the soil as described in Appendix C.

3.1.4 Characterisation of Soil Dynamics using Important Parameters

Effective thermal diffusivity of sand medium

The thermal diffusivity α of material is defined as $\alpha = \frac{k}{\rho c_p}$ which is a measure of heat transport, k relative to the energy storage, ρc_p. It is an important thermal transport property to determine the temperature response for transient conduction. As a corollary, the effective thermal diffusivity of the sand medium is then defined as $\alpha_{eff} = k_{eff} / (c_p \times \rho)_{eff}$. Likewise with most materials, the thermal diffusivity of the sand medium has a strong temperature dependence which decreases with increasing temperature.

Substituting k_{quartz} = 7 W/m.K, k_{air} = 0.03 W/m.K, $c_{p,air}$ = 1008 J/kg.K, $c_{p,quartz}$ = 815 J/kg.K, ρ_{air} = 1 kg/m^3, ρ_{quartz} = 2660 kg/m^3 (Incropera and DeWitts 1985) at T_{average} = 310K, the effective thermal conductivity of dry coarse and fine sands are estimated using the simple geometric mean method:

$$k_{eff,coarse} = \prod_{i=1}^{n} k_i^{v_i} = (7)^{0.52} \times (0.03)^{0.48} = 0.51 \text{ W/m.K}$$

$$k_{eff,fine} = \prod_{i=1}^{n} k_i^{v_i} = (7)^{0.6} \times (0.03)^{0.4} = 0.79 \text{ W/m.K}$$

The effective heat capacity of dry sands is given by:

For coarse sand,

$$(\rho c_p)_{eff} = \sum_{i=1}^{n} v_i \times (\rho c_p)_i = (0.52 \times 2660 \times 815) + (0.48 \times 1 \times 1008) = 1.128 \times 10^6 \text{ J/m}^3\text{.K}$$

For fine sand,

$$(\rho c_p)_{eff} = \sum_{i=1}^{n} v_i \times (\rho c_p)_i = (0.6 \times 2660 \times 815) + (0.4 \times 1 \times 1008) = 1.301 \times 10^6 \text{ J/m}^3\text{.K}$$

The overall effective thermal diffusivity of dry fine and coarse sand are then given by:

$$\alpha_{eff}(\text{coarse sand}) = \frac{k_{eff}}{(\rho c_p)_{eff}} = \frac{0.51}{1.13 \times 10^6} = 5 \times 10^{-7} \text{ m}^2/\text{s}$$

$$\alpha_{eff}(\text{fine sand}) = \frac{k_{eff}}{(\rho c_p)_{eff}} = \frac{0.79}{1.301 \times 10^6} = 6.1 \times 10^{-7} \text{ m}^2/\text{s}$$

These computed effective thermal diffusivity values for dry fine and coarse sand are useful as inputs to the 1-D analytical model developed to predict the response of dry soil medium heated from below. The results of the analytical model will be discussed in Chapter 4.

Definitions and relationships between Rayleigh number Ra, critical Rayleigh number Ra_{cr} and Nusselt number Nu

In the traditional domain of fluid mechanics, the Rayleigh number is a product of the Grashof number, $Gr = g\beta\Delta T H^3 / \upsilon^2$ which is a ratio between buoyancy and viscous forces and the Prandtl number, $Pr = \upsilon / \alpha$ which describes the relationship between momentum diffusivity and thermal diffusivity. Note υ is the fluid kinematics viscosity; g is the gravitational constant; T is the temperature; β is the coefficient of thermal expansion; H is the height dimension; α is the thermal diffusivity. In normal convection analysis, the Rayleigh number can be used to distinguish the two different regimes of heat transfer namely conduction and convection.

In geotechnics, the Rayleigh number is also a dimensionless number, which can be conceived as the ratio of the combined viscous and thermal diffusive time scales to the temperature-induced buoyancy time scale. Its definition is as follows:

$$Ra = \frac{g\lambda\beta(T_l - T_o)H}{\nu\left(\frac{k_e}{(\rho c_p)_f}\right)} \qquad (3.1)$$

Substituting the modified velocity scale v ~ $\sqrt{\frac{g\lambda\beta\,\Delta T}{H}}$ for porous medium into Eqn. (3.1), taking into consideration that the velocity occurring in the porous medium also depends on the ratio of the permeability against height:

$$Ra = \frac{\mathrm{v}^2 H^2}{\upsilon\alpha}$$

$$= \left(\frac{\mathrm{v}^2}{\upsilon}\right) \times \left(\frac{H^2}{\alpha}\right)$$

$$= \left(\frac{\mathrm{v}^2}{H^2}\right) \times \left(\frac{H^2}{\upsilon}\right) \times \left(t_{conduction}\right)$$

$$= \left(\frac{\mathrm{v}^2}{H^2}\right) \times \left(t_{viscous}\right) \times \left(t_{conduction}\right)$$

$$= \left(\frac{1}{t_{buoyancy}}\right)^2 \left(t_{viscous}\right) \times \left(t_{conduction}\right)$$

$$= \left(\frac{t_{viscous} \times t_{conduction}}{t_{buoyancy}{}^2}\right) \qquad (3.2)$$

Qualitatively speaking, convection cells occur in a given soil medium when the buoyancy acceleration time, $t_{buoyancy}$ is short compared to the combined time it takes for the fluid to be decelerated by viscosity, $t_{viscous}$, and the time it takes for heat to be diffused by conduction, $t_{conduction}$. As a result, this leads to the notion that there is a certain critical *Ra* number Ra_{cr} which will yield the onset of convection. It is then not unexpected that many authors (Horton and Rogers 1945, Lapwood 1948, Bau and Torrance 1982, Nield 1968) have used the criterion of a critical Rayleigh number Ra_{cr} to predict the onset of convection in a porous medium subjected to a temperature

change ΔT. If the *Ra* number is less than Ra_{cr}, heat is transferred by conduction only. The values of the critical Rayleigh number Ra_{cr} depends on the type of the boundary conditions imposed as shown in Table 2 (§ 2.2.2).

On the other hand, the Nusselt number *Nu* has been used traditionally in the heat transfer analysis of the thermal boundary layer and is equal to the dimensionless temperature gradient at the surface ($Nu = hL/k$). It provides a measure of the convective heat transfer occurring at the surface.

However, in geotechnics, the Nusselt number can also be conceived as a ratio of the total applied heat flux to the conduction heat flux in the absence of convection as exemplified by Eqn. (3.3). Hence, the Nusselt number is a useful indicator to measure how effective the heat transfer rate takes place in the soil medium compared to conduction, analogous to its applications in thermal boundary layers.

$$Nu = \frac{hL}{k} = \frac{h\Delta T}{\left(\frac{k_{eff}\Delta T}{H}\right)} = \frac{\dot{q}''_{applied}}{\left(\frac{k_{eff}\Delta T}{H}\right)} = \frac{\dot{q}''_{applied}}{\dot{q}''_{conduction}} \qquad (3.3)$$

In geotechnics, there has been much debate on how the Nusselt number will change with the Rayleigh number and this problem has not been resolved yet. Basically, it has been agreed that the Nusselt number will remain constant (=1) till the onset of the convection and it will rise steeply. From that point onwards, the Nusselt number *Nu* will then generally increase with increasing Rayleigh number. The relationship can be expressed as follows:

$$Nu = \mathrm{f}\left(\frac{Ra}{Ra_{cr}}, Pr\right) \tag{3.4}$$

A higher Nusselt number (>1) indicates a faster heat transfer rate induced by convection and/or boiling compared to pure conduction. As a result, there is a higher heat extraction rate from tunnel fires that is transmitted via the tunnel lining, resulting in lower temperature in the lining. It is interesting to note that Eqn. (3.4) is analogous to the functional dependence of the average Nusselt number in the traditional thermal boundary layer analysis: $Nu = \mathrm{f}(Re_L, Pr)$. Figure 13 shows the typical qualitative relationship between the Nusselt number *Nu* and Rayleigh number *Ra* in geotechnics.

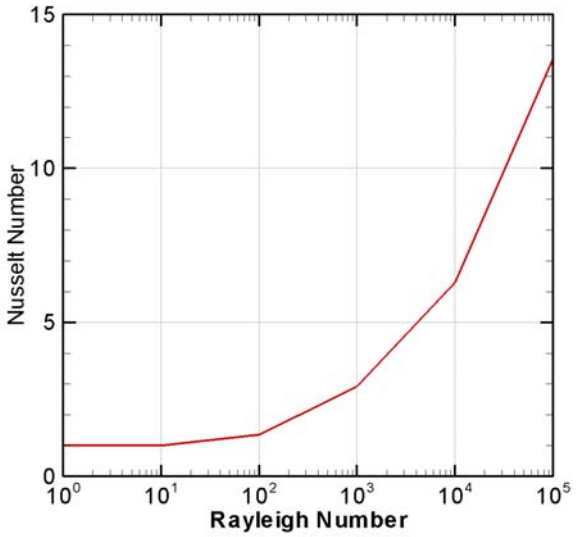

Figure 13. Typical qualitative dependence of *Nu* on *Ra*.

Speed of the propagating saturation temperature front

When a fully saturated porous media is subjected to sufficiently high heat flux to cause boiling to occur, another thermal transfer mode via the propagation of a saturation temperature front would be expected. This phenomenon constitutes an overlaying water layer at approximately room temperature, an intermediate region with temperature distribution that varies from ambient to saturation temperature over a short region and an underlying two-phase/boiling region at the thermal saturation temperature. The region of influence of the boiling region, though bounded by the overlaying water layer at ambient temperature, will grow progressively with time whilst the height of the upper water region will decrease. The height of the intermediate region remains relatively constant. The speed of the propagating saturation temperature front is important to determine the rate at which heat transfer takes place through the soil medium. For example, the faster the propagating speed, the higher will be the rate of vaporization of water and heat transfer rate, implying greater heat extraction rate from the fire, resulting in lower lining temperature and vice versa.

Maximum Temperature and Pore Water Pressure

Campanella and Mitchell (1968) observed that saturated soils subjected to temperature increase under undrained condition at constant effective stress could cause excess pore water pressure to build up significantly. Preliminary experiments with surcharge applied at the top, produced pore water pressure build-up as high as 2.06 bar (30 psi). However, since our experimental configuration is open to ambient

at the top and not closed, it is anticipated that the pore water pressure built up in the fully saturated soil medium during the intense heating will dissipate gradually with time to the environment through the top of the soil column. The rate of dissipation of the pore water pressure with time typically depends on the type of boundary conditions imposed and the permeability of the porous media. As a result, the maximum pore water pressure increase ΔP_{max} measured will be used to determine the critical soil behaviors/conditions affecting the lining stability during tunnel fires. There are two possible ways that the increased pore water pressure can affect the lining stability namely (1) it can contribute to the total stresses acting on the crown of the tunnel lining and (2) it can enhance the propensity of producing detrimental regions of discontinuity such as voids momentarily at the soil/lining interface during the venting of the pressure. It is highlighted in § 2.4 that the absence of support induced by presence of voids at the soil/lining interface poses one of the most serious problems for tunnel lining design. Similarly, the maximum temperature recorded during the experiments will give a measure of the possible critical impacts on the soil medium when exposed to such extreme temperature conditions, which in turn affects the lining stability.

Soil Channeling

Whenever boiling occurs simultaneously with increased pore water pressure, the bubbles produced will create pathways of least resistance in the soil medium to reach to the top for pressure venting and results in channels being created within the soil medium. Soil channeling is an important behavior that can adversely affect the

stability of the tunnel lining which depends on the contact continuity at the soil/lining interface because channeling could result in voids of discontinuity at the interface.

3.2 Description of the Experimental Setup

3.2.1 Improved Test Apparatus

A few significant improvements were made to the initial test apparatus which are enumerated in the following section. The discussion in this section will focus mainly on the description of current, improved test apparatus. The test apparatus consisted of a testing tube that was mounted to a frame made out of Bosch aluminum-profile-bars (refer to Figure 14). Moreover, the mounting frame was provided with four locking casters to allow easy movement of the hefty test apparatus from one work area to other. The drawing for the mounting frame is shown in Figure 15.

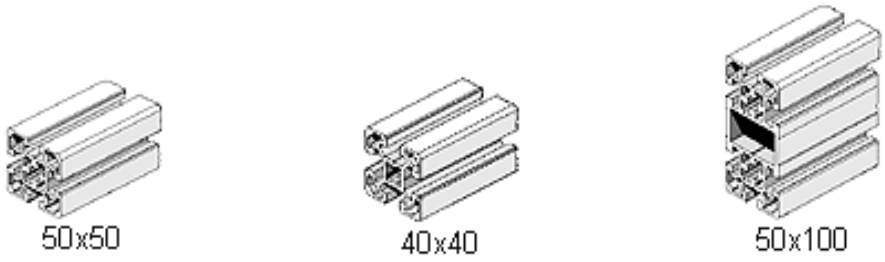

Figure 14. Bosch Aluminum Profiles (www.kjn-automation.co.uk).

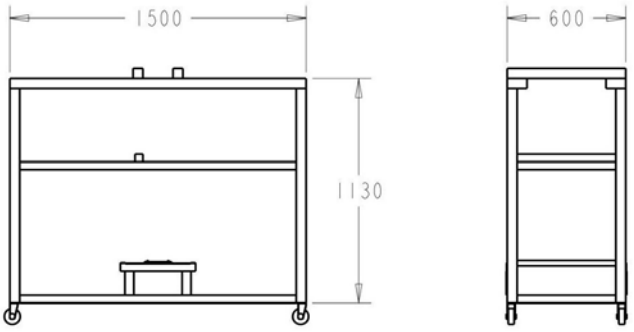

Figure 15. Drawing of the Mounting Frame (Paul 2004).

To enclose a cylindrical core of the soil specimen to be heated during the experiments, a testing tube was fabricated by riveting together one 4" diameter stainless steel plain beaker (McMaster Part# 4352T5) and two galvanized steel tubes (McMaster Part# 1766K12 and 1766K49) with a combined height of about 1500mm. One of the advantages of this test apparatus was that it could be assembled and taken apart easily any time, which in turn facilitated easier collection of soil specimens in the course of tube dissection after the experiments. Furthermore, the joints between the adjoining tubes were filled with RTV silicone and secured with tube clamps (McMaster Part# 45945K19) to provide a tight water seal, thus preventing water from leaking during the heating process.

The testing tube was then wrapped with 25 mm thick layer of fiberglass insulation throughout to eliminate lateral heat loss, thereby insuring a simplified one-dimensional heat transfer through the soil column in the tube. The testing tube was supported by two parallel L-shaped steel bars at the bottom and these bars were bolted to the frame. Furthermore, the tube was held tightly in position by aluminum profiles secured to the mounting frame at two different elevations. The entire test apparatus is shown in Figure 16.

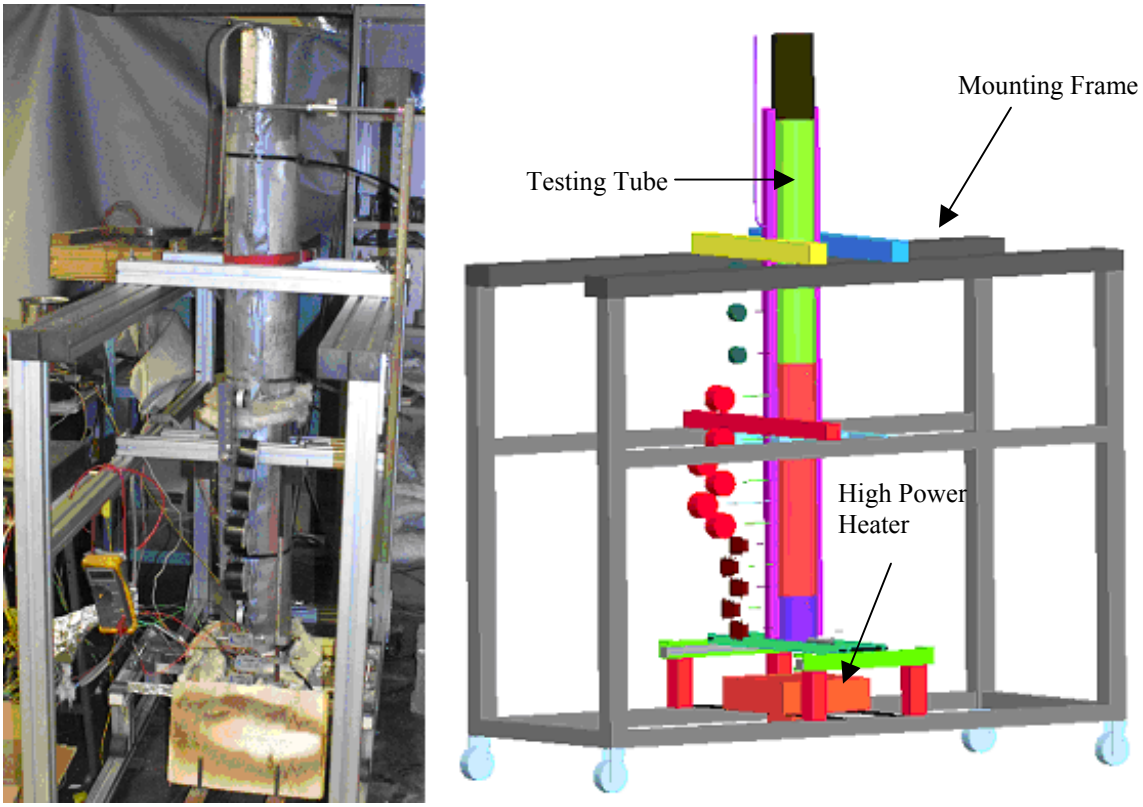

Figure 16. Improved test apparatus.

To produce fully saturated conditions for the soil medium, it is envisaged that water must be added but with the requirement that little air was entrapped during the filling process. Introduction of water from the bottom of the testing tube allowed the air in the soil medium to be expelled at the top. Water was gradually introduced by means of a high temperature three-piece ball valve (McMaster Part# 4632K243) shown in Figure 17, that was welded near to the base of the testing tube. The water level in the soil medium during the filling process was monitored through a transparent PVC pipe which extended from the ball value and up the side of the tube.

Figure 17. Three-Piece Ball valve (www.mcmaster.com).

A high power heater was placed about 4" below the base of the testing tube to provide the necessary high heat flux to heat up the soil medium. The high power heater (Omega Part# QH-101060-T) is a quartz infrared radiant panel heater shown in Figure 18 which was capable of providing a maximum heat flux of 90 kW/m^2 and a maximum temperature of about 1000°C at its quartz surface. This heater is robustly designed with its housing made of rugged aluminized steel with the electrical terminal housing on the back.

Figure 18. High Power Heater (www.omega.com).

A control circuit was also set up based on a temperature controller (OMEGA Part # CN8201-R1) to regulate the temperature through a thermocouple placed at the thermowell of the radiant heater. The schematic diagram for the control circuit is illustrated in Figure 19.

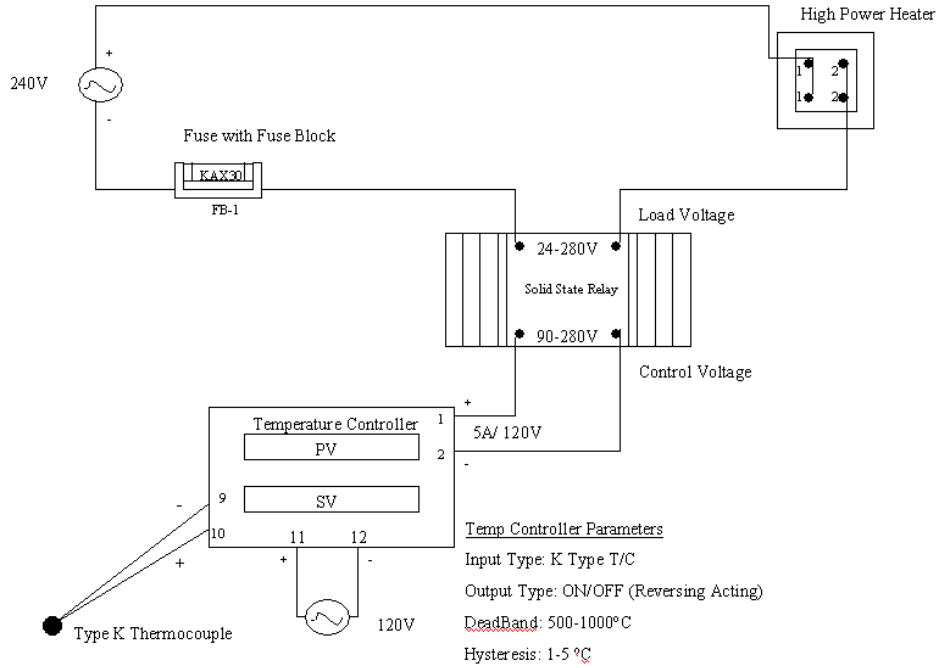

Figure 19. Schematic Diagram of the Temperature Control Circuit.

3.2.2 Instrumentation

Temperature Measurement

A total of sixteen thermocouples at different elevations were mounted at the side of the testing tube to measure the temperature in the center of the soil column. Each of the ten thermocouples closest to the bottom was positioned with a fixed distance of 50.8 mm between each other. The remaining six thermocouples closest to the top were placed at equal distance of 101.2 mm between each other. These thermocouples

were fabricated by inserting thin thermocouple wire (Omega Part# GG-K-36-SLE-200) through 1/16 “ diameter stainless steel pipes (McMaster Part# 51755K11) which were then attached to the testing tube using 1/16 “ Swagelok fittings (Swagelok Part # SS-100-1-OR). The ends of the stainless steel pipes outside of the tube were clamped using copper split-bolt connectors (McMaster Part# 6921K56) and sealed with RTV silicone to prevent water leakage even at appreciable high pressure. Subsequently, the thermocouples were connected to the PC via the NetDAQ data acquisition system to record the data measurements electronically. Another thermocouple (OMEGA Part # XCIB-K-4-1-3) was also attached to the bottom of the testing tube to measure the surface temperature at the base of the soil column. Furthermore, one quick disconnect thermocouple (OMEGA Part # KQSS-116U-12) was inserted into the thermowell of the heater to measure the temperature at the surface of the heater.

Pore Water Pressure Measurement

At the opposite side of the tube at the same elevations as the thermocouples, five pressure transducers (Omega Part# PX242A-005G5V) and nine pressure gauges (McMaster Part# 4026K2 and 4000K717) were attached to the tube using 1/16 ” and 1/8 ” Swagelok fittings to measure the pore water pressure. The pressure transducers and the pressure gages are shown in Figure 20. The readings of pressure transducers were also recorded electronically using the NetDAQ data acquisition system. Furthermore, a compact regulated power supply unit (OMEGA Part # PST-4130) shown in Figure 21 was used to provide regulated 8V input to the pressure transducers.

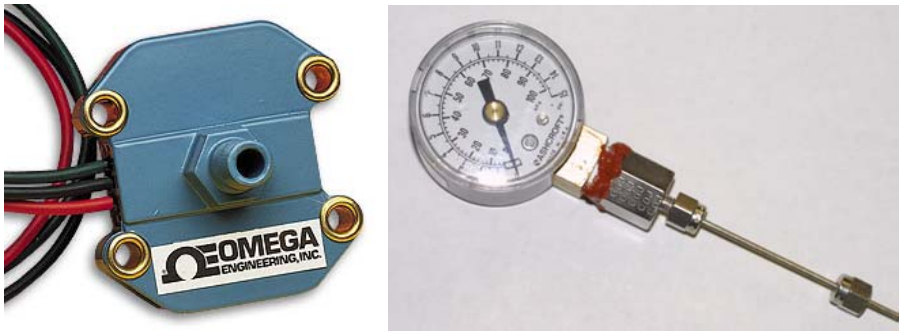

Figure 20. Pressure transducer and pressure gage (www.omega.com).

Figure 21. Compact regulated power supply (www.omega.com).

Volume Measurement

A clear plastic pipe with graduated markings was attached to the testing tube at a height of 1016 mm from the bottom. It was used to measure the change in the height of the water within the tube during the heating process. The configuration for the array of instrumentation used in the test apparatus is depicted in Figure 22.

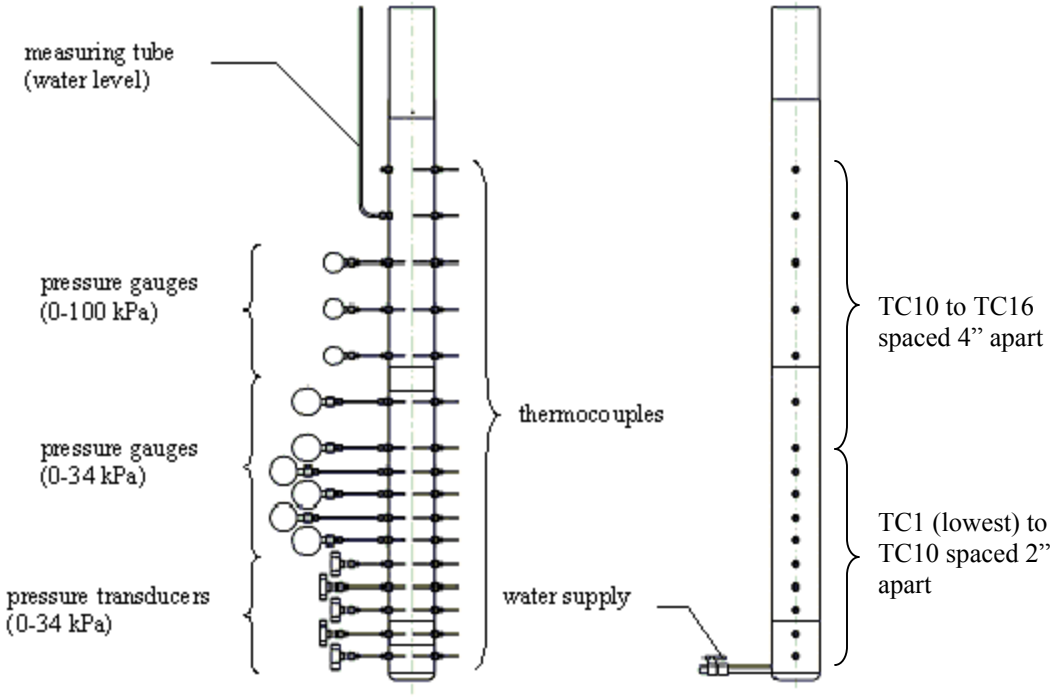

Figure 22. The instrumentation configuration (Note that TC represents thermocouple)

Data Acquisition

The measurements taken from the thermocouples and pressure transducers were captured electronically via the NetDAQ 2640A data acquisition unit (shown in Figure 23) and transmitted to the PC. The data was then recorded and consolidated into a data file. Each NetDAQ has 20 channels, which may be programmed individually to perform virtually any signal conditioning function the user requires.

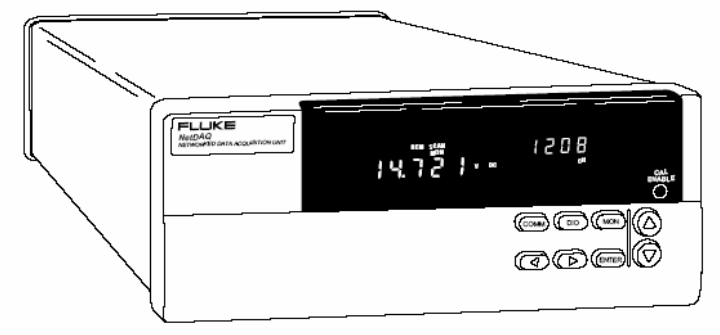

Figure 23. NetDAQ data acquisition unit (www.fluke.com).

3.2.3 Initial and Boundary Conditions

Specific boundary conditions were prescribed and implemented in the experimental configuration, taking into consideration the importance to reflect realistically the actual ground conditions:

(1) The top of the column was open to the ambient air (permeable and constant pressure) and the bottom end was closed (impermeable).

(2) The vertical walls of the tube bounding the soil column were watertight and impermeable.

(3) The temperature of the heater was set at approximately 750^{o}C using the temperature controller to simulate the extreme temperature conditions experienced during severe tunnel fires.

(4) The insulated walls of the tube could be assumed to be approximately adiabatic, with negligible heat loss. Therefore, it is assumed that the dominant direction of heat transfer in the experimental configuration is one-dimensional and vertical.

(5) The temperature of the soil medium before the commencement of any experiment is always taken to be at ambient condition ($\approx$ 25^{o}C).

(6) The configuration is assumed to follow the semi-infinite solid model because of the low aspect ratio. The temperature at the top of the soil medium is assumed to be at ambient ($\approx$ 25^{o}C) until the saturation temperature front reached the top.

3.2.4 Improvements Made to Initial Test Apparatus

Better Insulation Design

It was found that the thick and hotter stainless steel (SS) tube used in the original test apparatus to hold the soil specimen was transferring heat laterally to the colder soil specimen since steel has a higher conductivity compared to soil. As a result, the glass wool insulation was installed inside the SS tube to prevent any heat loss or gain. However, this method posed another difficulty - to design the insulation to be waterproof during the experiments involving fully saturated soil. Many techniques had been employed to insure that the insulation was waterproof but the higher temperature involved compounded the problem. It was virtually impossible to achieve a 100% waterproof condition for the insulation. Consequently, the testing tube was redesigned in the improved test apparatus to incorporate external placement of the glasswool insulation which eliminated this difficulty.

Improved Thermocouple Configuration

Initially, a wire was attached to the center of the bottom flange with a screw and extended vertically to the top of the tube. The thermocouple wires (Omega Part# GG-K-24-SLE) were attached to the wire at different elevations and similarly, extended to the top of the tube where they were connected to the data acquisition unit. Figure 24 illustrates the original configuration with the thermocouples attached to the center wire.

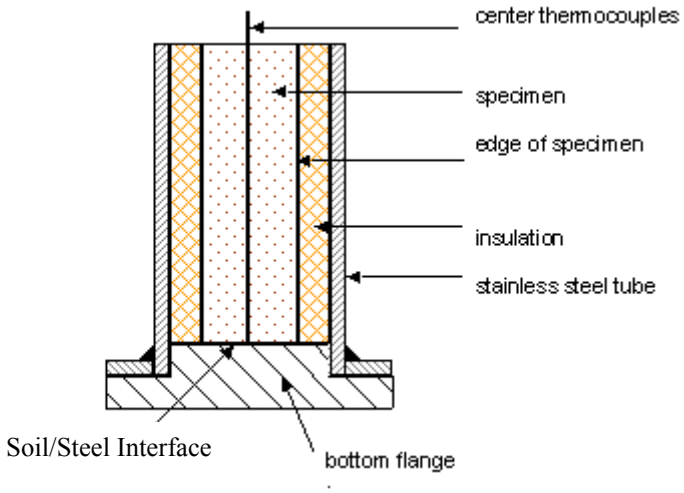

Figure 24. Original center thermocouple configuration (Gehrig 2004).

However, it was found that this method created a vertical pile of wires, at the center of the tube, which extended from the bottom to the top of the soil column. This vertical pile presented an "artificial" conduit or passageway which permitted easier movement of water within the soil medium and inadvertently catalyzed the convection cells to occur much more easily throughout the soil column, thus resulting in experimental results that did not represent the actual ground response. Eventually, the thermocouple configuration was revamped to eliminate this unintended consequence.

More Flexible Redesigned Testing Tube

One of the greatest advantages of the redesigned testing tube was that the ease of assembling and taking apart the three constituent tubes, which in turn facilitated easier collection of soil specimens during the tube dissection after the experiments. The thickness of the improved testing tube was also much smaller, thus reducing the magnitude of the lateral heat transfer to the soil specimen.

CHAPTER 4: RESULTS AND DISCUSSIONS

In this chapter, the experimental results for different soil types and conditions are shown. Preliminary analysis is then carried out to account for the expected transient behaviors of soil medium when subjected to extreme heat. In addition, critical dimensionless parameters such as Rayleigh and Nusselt numbers are demonstrated to adequately characterize the behaviors of soils. There is also some qualitative discussion on the potential impact on the stability of the tunnel lining due to these specific geotechnical behaviors.

4. 1 Experimental Results

4.1.1 The Response of Dry Soil Subjected to High Heat Flux

Referring to Figures 25(a) and (b), it is observed that the temperatures of dry coarse and fine sand heated from below show relatively gradual rise with time, indicating heat is transferred via pure conduction. Earlier experimental results have confirmed that the addition of thick glass wool insulation is sufficient to prevent substantial heat loss since the temperature difference between the outside surface and center of the tube is established to be negligibly small. Therefore, the assumption of a simple 1-D heat transfer is reasonable in our experimental configuration.

By dividing the entire soil column into equidistant nodes, an analytical model based on semi-infinite 1-D heat transfer and employing the *Crank-Nicholson implicit finite difference method* described in § 2.2.1, has been developed to predict the response of

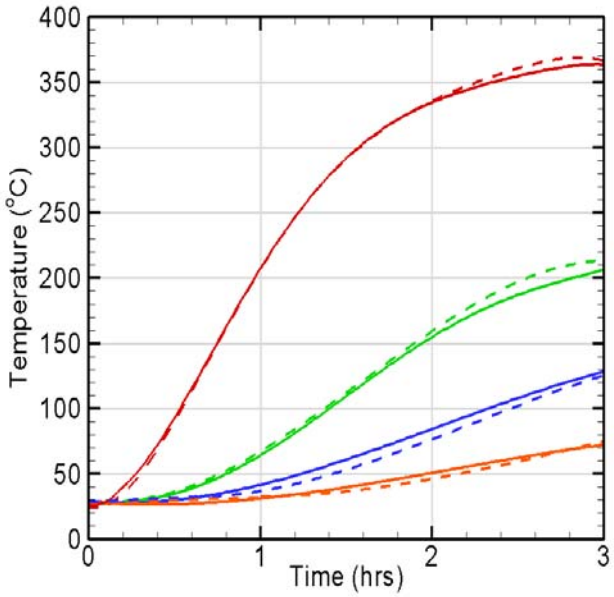

Figure 25(a). Comparison of analytical and experimental temperature profile of dry coarse sand (Note: TC1 stands for thermocouple 1 and so on). —— Experimental; ----- Analytical; —— TC1; —— TC2; —— TC3; —— TC4.

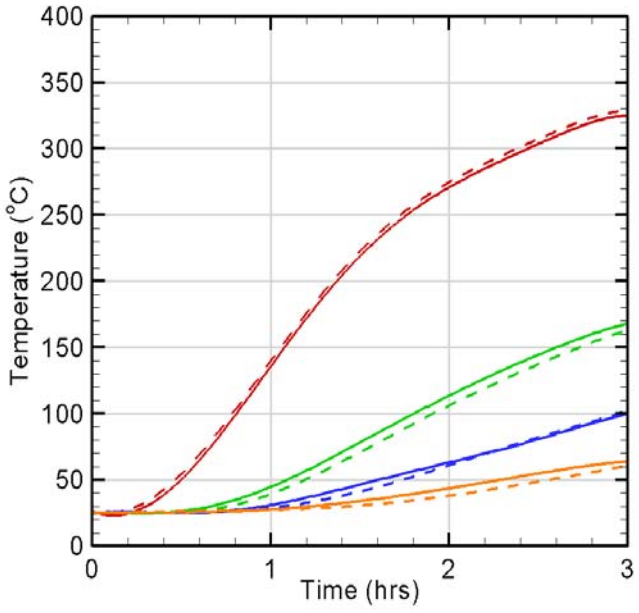

Figure 25(b). Comparison of analytical and experimental temperature profile of dry fine sand.—— Experimental; ----- Analytical; —— TC1; —— TC2; —— TC3; —— TC4.

dry soil heated from below. This model is designed to incorporate time-dependent temperature boundary conditions and effect of lateral heat transfer from the heated tube. It is postulated that the stainless steel tube holding the soil medium could heat up faster than the soil, and thus transfer some of the heat laterally to the soil. The effect of lateral heat transfer is included in the model by adding the term (h x ΔT) to every equation in the system of linear equations, where h is the lateral heat transfer coefficient, determined empirically by getting the best-fitting curves.

The temperature variation of the effective thermal diffusivity is also taken into account in the model. The model is written in FORTRAN Code and Gauss-Seidel Method is employed to find the solution of a linear system of equations. Subsequently, it is found that there is very good agreement between the actual and the predicted behaviors using the values of the effective thermal diffusivity for dry coarse and fine sand computed in §3.1.4 which are 5×10^{-7} and 6×10^{-7} m^2/s respectively.

Therefore, the behavior of dry soil subjected to extreme heating in the experimental soil column configuration follows closely that of a semi-infinite 1-D model with a fixed surface temperature applied at the bottom. It is postulated that the small discrepancy between theoretical and experimental results arises because the temperature dependence of the effective thermal diffusivity at each location is approximated based on the average temperature and applied over the entire temperature range. The response is therefore considered predictable, and completely compatible with existing theory of simple conductive heat transfer.

4.1.2 The Response of Fully Saturated Soil Subjected to High Heat Flux

Figures 26(a) and 26(b) indicate that saturated soil behavior when heated is markedly different from that of dry sand. When a water-saturated soil medium is exposed to high heat flux, the entire column during heating is divided into three zones namely an overlaying cold water at ambient temperature where heat transfer is dominated by conduction, an intermediate zone characterized by a temperature gradient where heat is transferred by either by convection or conduction, and an underlying two-phase layer at approximately saturation temperature ($\approx 100^{o}C$) with counter-percolating flow of liquid and vapor. Figure 26(a) illustrates explicitly the development of these three distinct regions in fully saturated fine sand when heated. It can be inferred from the linear temperature gradients that conduction dominates the heat transfer within the intermediate zone for fully saturated fine sand. There is also perceptible upward propagation of a saturation temperature front ($\approx 100^{o}C$) through the soil column at the onset of boiling. Moreover, the underlying two-phase zone remains essentially isothermal at the saturated temperature during the propagation of the saturation temperature front.

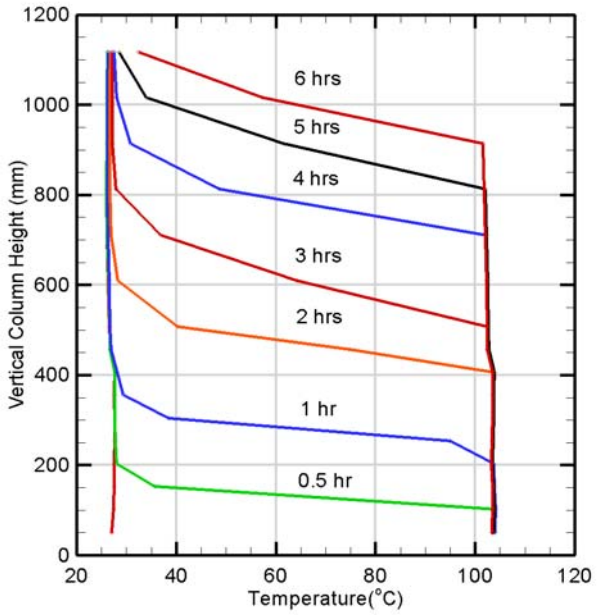

Figure 26(a). Temperature profile of fully saturated fine sand heated from below.

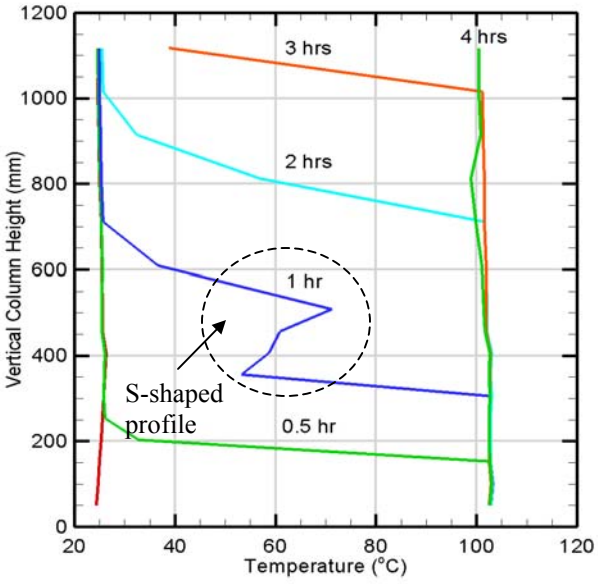

Figure 26(b). Temperature profile of fully saturated coarse sand heated from below.

As shown in Figure 26(b), fully saturated coarse sand of higher permeability exhibit similar behaviors when heated except that convection appears to be the dominant heat transfer mechanism in the intermediate zone, identified by the distinctive S-shaped temperature profile (Bau and Torrance 1982). There was no convection occurring after 2 hours because the convection cell was superseded by the saturation temperature front. It has been found that the differences in mechanisms of heat transfer for identical experimental boundary conditions are attributed to differences in soil properties. The development or suppression of S-shaped curves signaling significant convection in the pore water is influenced by soil permeability and the details will be discussed in subsequent sections.

Furthermore, the propagating speeds of the saturation temperature front in fully saturated coarse and fine sand are determined to be approximately 300~400 mm/hr and 100~200 mm/hr respectively, differing by a factor of about 2. It is believed that the rate of propagation of the saturation temperature front is affected by two factors namely (1) the relative proportions of water and soil solids in the saturated soil which is secondary; and (2) the mechanisms of heat transfer. Albeit the thermal diffusivity values for fully saturated coarse and fine sand, which depend on the relative proportion of water and soil solids, are different (~30%), experimental results suggest that the onset of convection is pivotal in engendering a much faster rate of heat transfer in the soil column, which accounts for the significant difference in the propagating speeds of the saturation temperature front in fully saturated coarse and fine sand. In the fine sand with saturated unit weight averaging 2000 kg/m^3, the ratio

of volume of water to volume of soil particles will be 2:3. In the coarse sand with saturated unit weight averaging 1830 kg/m^3, the ratio of volume of water to volume of soil particles will be 1:1.

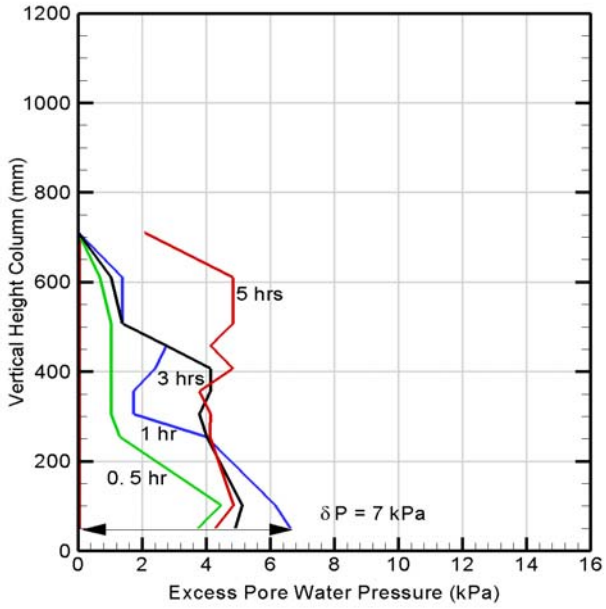

Figure 27(a). Excess pore water pressure profile of fully saturated fine sand heated from below.

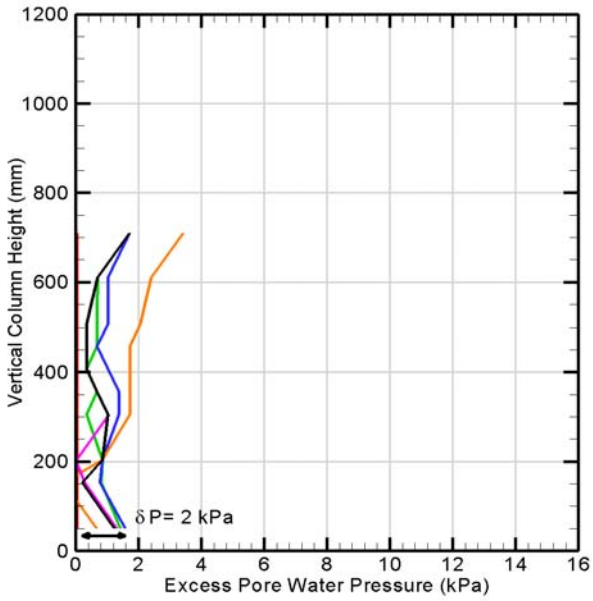

Figure 27(b). Excess pore water pressure profile of fully saturated coarse sand. 0.5 hr; 1 hr; 2 hrs; 3 hrs

In addition, Figures 27(a) and (b) demonstrate that excess pore water pressure building up in fine sand (7~14 kPa) is also higher than that in coarse sand (2~8 kPa), Again, this is attributed to differences in permeability that allowed development of convection in the pore water in coarse soil, and less pressure build-up, than in fine soil where movement of water is less readily developed.

4.1.3 The Response of Partially Saturated Fine and Coarse Sand

Figures 28(a) and (b) indicate that the dominant mode of heat transfer through partially saturated soil is by conduction and boiling manifested in the propagation of the saturation temperature front through the soil column at the onset of boiling. There is no observable development of convection cells in either the partially saturated coarse sand or the partially saturated fine sand. As for the saturated case, the speed of propagation is greater in the more permeable coarse sand (400~500 mm/hr) than in the fine sand (200~300 mm/hr) by a factor of roughly 2, but in both cases, the speeds of propagation are much greater than occurred in the same soils when they were saturated. Differences between the saturated and the partially saturated cases are attributed to the lesser amount of water available to be heated in the partially saturated soil. As for the saturated cases, the underlying two-phase zone remains essentially isothermal at the saturated temperature during the propagation of the saturation temperature front.

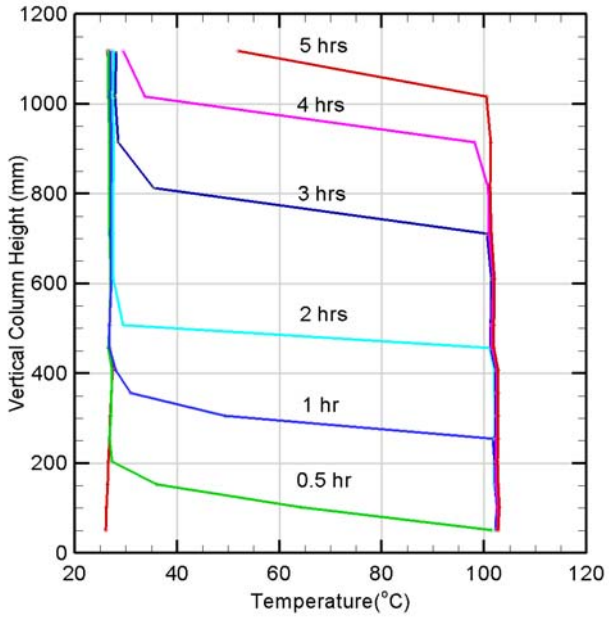

Figure 28(a). Temperature profile of partially saturated fine sand heated from below.

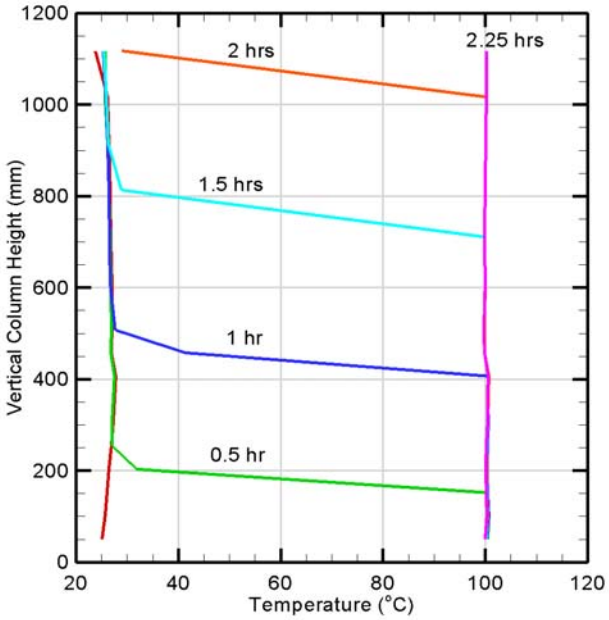

Figure 28(b). Temperature profile of partially saturated coarse sand heated from below.

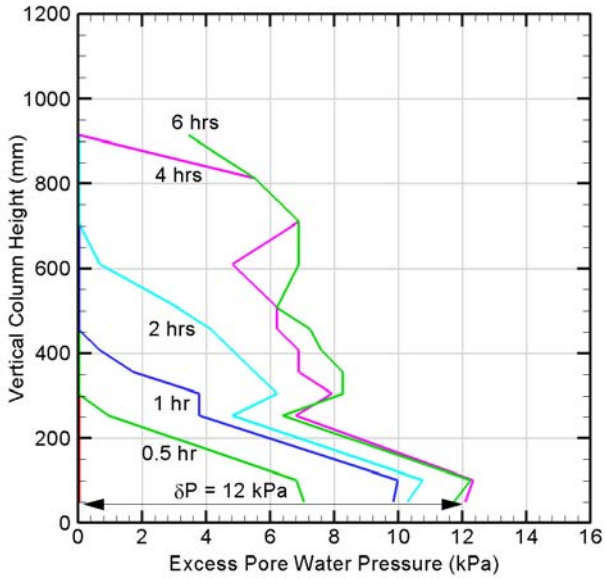

Figure 28(c). Excess pore water pressure profile of partially saturated fine sand.

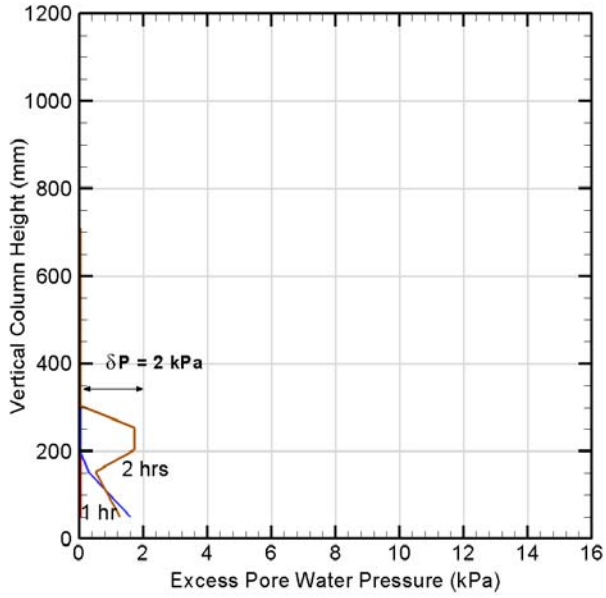

Figure 28(d). Excess pore water pressure profile of partially saturated coarse sand.

Similarly, Figures 28(c) and (d) demonstrate that excess pore water pressure building up in partially saturated fine sand is greater than that measured in partially saturated coarse sand. This is attributed, as before, to the greater permeability of the coarse sand that permits more effective dissipation of thermally generated pore water pressures than in the fine sand.

4.1.4 The Response of Fully Saturated Silt Subjected to High Heat Flux

Figures 29(a) and (b) show the experimental results for fully saturated silt. The results indicate some marked differences. First, convection occurs in saturated silt before the onset of boiling, unlike that observed in the behaviors for saturated fine and coarse sand. Second, there is no upward propagation of a saturation temperature front through the silt column as the onset of boiling appears to occur simultaneously throughout the silt column, although that behavior is observed in the saturated fine sand immediately above the silt. It is postulated that the more vigorous convection occurring in silt permits more effective heat exchange throughout the entire silt column resulting in a temperature gradient that pervades the entire silt column, as opposed to the three-layer system observed in fully saturated sands, which explains why the onset of boiling occurs simultaneously throughout the silt column.

It is noteworthy that the excess pore water pressure building up in the fully saturated silt (25~40kPa) is appreciably higher than that experienced in fully saturated fine or coarse sand, obviously due to its much lower permeability which does not allow pore water pressure to be dissipated as easily. Hence, notwithstanding the development of S-shaped convection temperature profiles observed for these saturated silt tests, there is strong evidence that pressure-driven flow instead of buoyancy, is primarily responsible for the occurrence of the convection cells in silts. The fact that the height of the silt column was only 500 mm, rather than the full column height for practical reasons associated with soil placement in the column, is believed to affect pore water pressure development, pore water pressure dissipation and mechanisms of heat

transport. These will be investigated in forthcoming experimental research with full height silt columns.

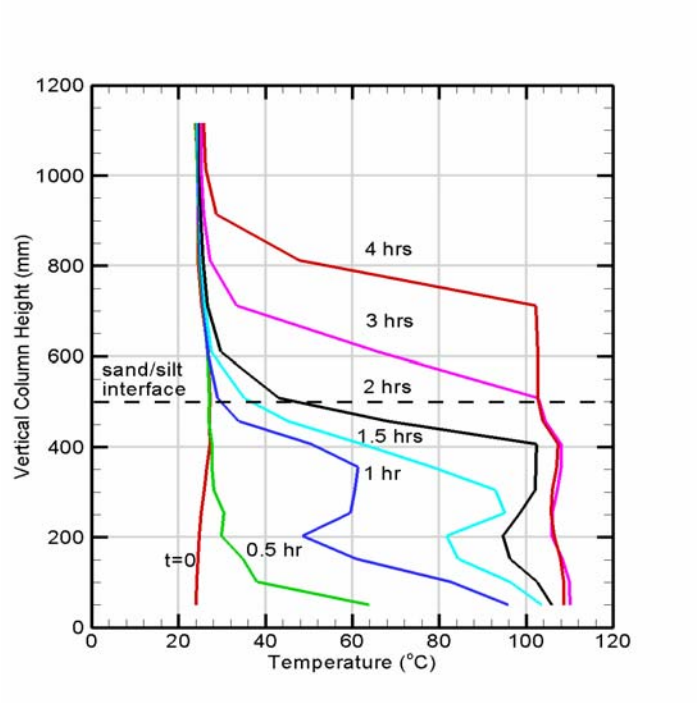

Figure 29(a). Temperature profile of fully saturated silt heated from below.

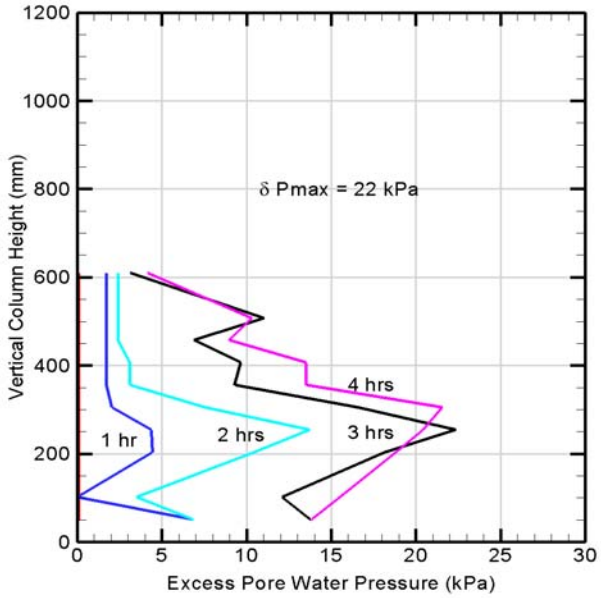

Figure 29(b). Excess pore water pressure profile of fully saturated silt heated from below.

4.2 Discussions

4.2.1 Transient Convection and Boiling Phenomena in Fully Saturated Soils Subjected to High Heat Flux

Although existing established methods have been developed by several authors (§ 2.2.2 and 2.2.3: Bau and Torrance 1982, Nield and Bejan 1999) using the Rayleigh number as a criterion to predict the onset of convection under steady-state conditions, they are inadequate to describe the response of soil to transient-state conditions which is a better representation of the actual ground conditions encountered in tunnel fires. Consequently, a novel approach (adapted from Tan and Thorpe, 1996) is adapted to explain the transient behavior of saturated soils subjected to high heat flux. Experimental results for saturated coarse sand indicate that the onset of convection occur after the onset of boiling and propagation of the saturation temperature front. Essentially, the entire column during heating is divided into three zones namely the overlaying cold water at ambient temperature where heat transfer is dominated by conduction, the intermediate zone characterized by a temperature gradient where heat is transferred either by convection or conduction, and an underlying two-phase layer with counter-percolating flow of liquid and vapor. Taking a control volume of one snapshot of the propagating saturation temperature front as depicted in Figure 30,

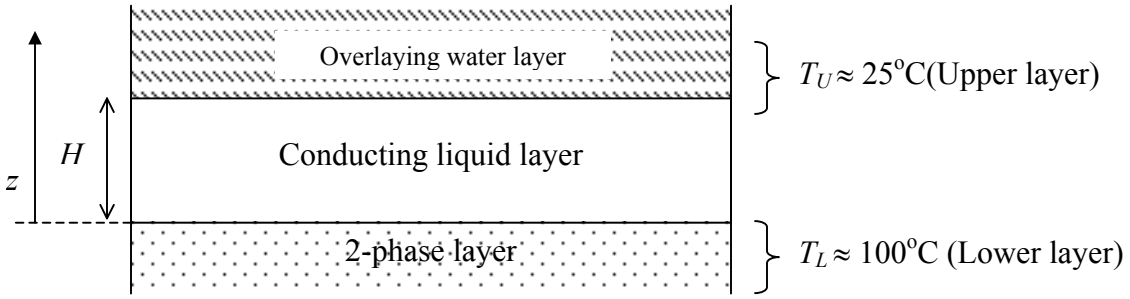

Figure 30. Control volume of propagating saturation temperature front in a saturated porous medium.

We define the transient Rayleigh Number as given by:

$$Ra_{transient} = \frac{g\lambda\beta z^2}{\nu\left(\frac{k_e}{\rho_f c_{pf}}\right)}\left(\frac{\partial T}{\partial z}\right), \quad z<H \tag{4.1}$$

where k_e is the effective thermal conductivity of the soil medium, ν is the kinematic viscosity of fluid, g is the gravitational constant, λ is the soil permeability, β is the coefficient of thermal expansion of fluid, ρ_f is the fluid density and c_{pf} is the specific heat capacity of fluid.

The temperature profile for the conducting liquid layer with the *constant lower temperature* at 100°C before the onset of convection, is predicted using the analytical solution for semi-infinite solid with constant surface temperature as described by Eqn. (4.2).

$$\frac{T_L - T}{T_L - T_U} = erfc\left(\frac{z}{2\sqrt{\alpha_m t}}\right) \tag{4.2}$$

If we differentiate Eqn. (4.2) w.r.t. z, we get:

$$\frac{\partial T}{\partial z} = \frac{\partial T}{\partial \eta} \times \frac{\partial \eta}{\partial z} = \frac{\Delta T}{\sqrt{\pi \alpha_m t}} e^{-\frac{z^2}{4\alpha_m t}} \quad \text{where } \eta = \left(\frac{z}{2\sqrt{\alpha_m t}} \right) \tag{4.3}$$

Substituting Eqn. (4.3) into Eqn. (4.1):

$$Ra_{transient} = \frac{g\lambda\beta z^2}{\nu\left(\frac{k_e}{\rho_f c_{pf}}\right)} \left(\frac{\partial T}{\partial z} \right) = \frac{g\lambda\beta z^2}{\nu\alpha_m} \left(\frac{\Delta T}{\sqrt{\pi \alpha_m t}} e^{-\frac{z^2}{4\alpha_m t}} \right), \quad z<H \tag{4.4}$$

To determine the position z^* at which the Rayleigh number attains a maximum, we can differentiate Eqn. (4.4) further:

$$\frac{\partial Ra}{\partial z} = 0$$

$$\Rightarrow \quad \frac{g\lambda\beta}{\nu\alpha_m} \left(\frac{\Delta T}{\sqrt{\pi \alpha_m t}} e^{-\frac{z^2}{4\alpha_m t}} \right) \left[2z - \frac{z^3}{2\alpha_m t} \right] = 0$$

$$\Rightarrow \quad z^* = 2\sqrt{\alpha_m t}$$

Substituting $z = 2\sqrt{\alpha_m t}$ into Eqn.(4.4) and knowing that Ra_{cr}(theoretical) = 27.10 based on impermeable conducting bottom surface and permeable conducting upper surface, results in the following expression:

$$\left(Ra_{transient}\right)_{\max} = \frac{g\lambda\beta\, 4\sqrt{\alpha_m t}}{\nu\left(\frac{k_e}{\rho_f c_{pf}}\right)} \left(\frac{\Delta T}{\sqrt{\pi}} e^{-1} \right) = \mathrm{Ra_{cr}} = 27.10$$

$$\Rightarrow \quad t_c = 1066 \times \left(\frac{\upsilon\sqrt{\alpha_m}}{g\lambda\beta\Delta T} \right)^2 \quad \text{where } t_c\text{: time to onset of convection}$$

$$\Rightarrow \quad \boxed{t_c \, \alpha \, \frac{\alpha_m}{\lambda_{soil}^{\,2}}} \tag{4.5}$$

Eqn. (4.5) is useful in that it suggests that t_c is independent of the column height and depends only on soil constituents that affect α_m and permeability λ_{soil}, assuming other parameters are constant. Therefore, $z^* = 2\sqrt{\alpha_m t_c}$.

Upon differentiating $z^* = 2\sqrt{\alpha_m t}$ w.r.t time, we get $\frac{\partial z^*}{\partial t} = \sqrt{\frac{\alpha_m}{t}}$. This quantity, $\frac{\partial z^*}{\partial t}$ can be conceived as the speed at which the convection front will propagate under transient conditions. Subsequently, it is postulated that the development of convection, identified by the distinctive S-shaped temperature profile, appears to depend on the competing influences of two velocity scales governing the propagation of the saturation temperature front and the onset of convection.

Substituting the following values at T_{fluid} = 350 K (Incropera and DeWitt 1985), $\beta(H_20) = 652.3x10^{-6}/K$; $\nu(H_20) = \mu/\rho = 343x10^{-9}$ kg m^2/s; k_e= 2~3 W/m.K; ρ_f =1000 kg/m^3 ; C_{pf}= 4195 J/kg-K; ΔT= 75 K; $\lambda_{fine} = 7.2\times10^{-11}\,m^2$; $\lambda_{coarse} = 2.3\times10^{-9}\,m^2$.

<u>For fully saturated coarse sand</u>

$\frac{\partial z^*}{\partial t} = \sqrt{\frac{\alpha_m}{t}} = \sqrt{\frac{2.2}{1000\times4195}} = 9.42\times10^{-2}\,mm/s$, which can be conceived as the speed at which the convection front will propagate. Experimental results showed that the saturation temperature front in fully saturated coarse sand propagates at 8.3 x 10^{-2} ~ 11 x 10^{-2} mm/s. If the speed of the propagation for the saturation temperature front exceeds the convection cells for instance, under high heat flux, the boiling mechanism will supercede and dampen out the development of the convection cells. Similarly,

convection will be generated in coarse sand if the speed of convection front is higher than that of the saturation temperature front. This provides a reasonable basis to explain why a moderate heat flux spawns more vigorous convection cells compared to that produced under high heat flux.

For fully saturated fine sand

$\frac{\partial z^*}{\partial t} = \sqrt{\frac{\alpha_m}{t}} = \sqrt{\frac{\frac{2.8}{1000 \times 4195}}{21 \times 3600}} = 3.0 \times 10^{-3}\, mm/s$. Experimental results showed that the saturation temperature front in fully saturated fine sand propagates at 2.7 x 10^{-2} ~ 5.6 x 10^{-2} mm/s. The upshot of this method predicts that the saturation temperature front will supercede and dominate in fully saturated fine sand before the convective cells have the chance to develop, which is found to be consistent with the experimental observations.

For silt

Similarly, using the definition of the transient Rayleigh Number as given by:

$$Ra_{transient} = \frac{g\lambda\beta z^2}{\nu\left(\frac{k_e}{\rho_f c_{pf}}\right)}\left(\frac{\partial T}{\partial z}\right), \quad z<H$$

Since the convection occurs before the onset of boiling in the case for fully saturated silt, the approach has to be modified for constant heat flux. Hence, the temperature profile for the conducting liquid layer with the *constant heat flux* before the onset of

convection and boiling, can be predicted using the analytical solution (Carslaw and Jaeger, 1986) for semi-infinite stationary fluid as described by Eqn. (4.6).

$$T_i - T = \frac{2\dot{q}''\sqrt{\alpha_m t}}{k_{eff}} ierfc\left(\frac{z}{2\sqrt{\alpha_m t}}\right) \tag{4.6}$$

If we differentiate Eqn. (4.6) w.r.t. z, we get:

$$\frac{\partial T}{\partial z} = \frac{\partial T}{\partial \eta} \times \frac{\partial \eta}{\partial z} = -\frac{\dot{q}''}{k_{eff}} erfc\left(\frac{z}{2\sqrt{\alpha_m t}}\right) \quad \text{where } \eta = \left(\frac{z}{2\sqrt{\alpha_m t}}\right) \tag{4.7}$$

Substituting Eqn. (4.7) into Eqn. (4.1):

$$Ra_{transient} = \frac{g\lambda\beta z^2}{\nu\left(\frac{k_e}{\rho_f c_{pf}}\right)}\left(\frac{\partial T}{\partial z}\right) = \frac{g\lambda\beta z^2}{\nu\alpha_m}\left(\frac{\dot{q}''}{k_{eff}} erfc\left(\frac{z}{2\sqrt{\alpha_m t}}\right)\right), \quad z<H \tag{4.8}$$

To determine the position z^* at which the Rayleigh number attains a maximum, we can differentiate Eqn. (4.8) further:

$$\frac{\partial Ra}{\partial z} = 0$$

$$\Rightarrow \quad \frac{g\lambda\beta\dot{q}''z}{k_{eff}\nu\alpha_m}\left(2erfc\left(\frac{z}{2\sqrt{\alpha_m t}}\right) - \frac{z}{\sqrt{\pi\alpha_m t}} e^{-\frac{z^2}{4\alpha_m t}}\right) = 0$$

$$\Rightarrow \quad z^* = 1.684\sqrt{\alpha_m t}$$

Substituting $z^* = 1.684\sqrt{\alpha_m t}$ into Eqn.(4.8) and knowing that Ra_{cr}(theoretical) = 27.10 based on impermeable conducting bottom surface and permeable conducting upper surface yield:

$$\left(Ra_{transient}\right)_{\max} = \frac{g\lambda\beta\,\dot{q}'' \times 2.836\alpha_m t}{k_e \nu\left(\frac{k_e}{\rho_f c_{pf}}\right)}(0.23337) = \mathrm{Ra_{cr}} = 27.10$$

$$\Rightarrow \qquad t_c = 40.9 \times \left(\frac{k_e \nu}{g\lambda\beta\dot{q}''}\right) \text{ where } t_c\text{: time to onset of convection}$$

$$\Rightarrow \qquad \boxed{t_c \;\alpha\; \frac{k_e}{\dot{q}''\lambda_{soil}}} \qquad (4.9)$$

Similarly, Eqn. (4.9) suggests that the onset of convection is independent of the column height and depends only on soil constituents, the permeability λ_{soil} and magnitude of heat flux.

Substituting the following values at T_f = 350 K(Incropera and DeWitt 1985) in Eqn. (4.9):

$\beta(H_20) = 652.3\text{x}10^{-6}$/K ; $\nu(H_20) = \mu/\rho = 343\text{x}10^{-9}$ kg.m^2/s; k_e= 3.2 W/m.K; ρ_f =1000 kg/m^3 ; C_{pf}= 4195 J/kg-K; $\dot{q}'' = 33$ kW/m^2; $\lambda_{silt} = 1\times10^{-11}$ m^2.

$$t_c = 40.9 \times \left(\frac{3.2 \times 343 \times 10^{-9}}{9.81 \times 1 \times 10^{-11} \times 652.3 \times 10^{-6} \times 33 \times 10^3}\right) = 5.9 \text{ hrs}$$

>> 0.5 hrs (observed from experiment)

This transient approach based on Rayleigh No. predicts that there is little likelihood for convection to occur in silt, however the experimental result has proven otherwise. Hence, it is postulated that this concept is no longer valid when the built-up pore water pressure becomes so significant that it drives the convection predominantly in the fully saturated silt compared to the weaker temperature-induced buoyancy forces.

Examining the momentum equation governing the fluid in porous media as given by:

$$\gamma_a \frac{\partial \hat{\boldsymbol{v}}}{\partial t} = -\nabla \hat{P} \quad - \hat{\boldsymbol{v}} \quad + Ra\hat{T}\boldsymbol{e}_z \tag{4.10}$$

where $\mathrm{Pr}_m = \mu / \rho_o \alpha_m$; $\boldsymbol{e_z}$ is the unit vector in the z-direction; $\boldsymbol{v}$ is the velocity vector;

$$\gamma_a = \frac{c_a \lambda}{\sigma \mathrm{Pr}_m H^2} \; ; \; Ra = \frac{\rho_o g \beta \lambda H \Delta T}{\mu \alpha_m} ; \; \hat{\boldsymbol{v}} = \frac{H\boldsymbol{v}}{\alpha_m} ; \; \hat{P} = \frac{kP}{\mu \alpha_m} \text{ and } \; \hat{T} = \frac{T}{\Delta T} .$$

The Boussinesq approximation where $\rho_f = \rho_o \left[1 - \beta\left(T - T_o\right)\right]$ is no longer valid in the case of fully saturated silt when the component from the pore water pressure cannot be neglected. Thus, the approach of using the critical Rayleigh number, based on the aforesaid assumptions, to predict the onset of convection in silt, is no longer valid.

4.2.2 Transient Behaviors in Partially Saturated Soils Subjected to High Heat Flux

As substantial amounts of water have been drained from soils to yield a partially saturated condition (saturation S ~ 0.3 to 0.7), there is no interconnectivity between the pore water whereby the limited amount of water left is inadequate to constitute

convection. Therefore, there is no discernible convection observed in partially saturated fine and coarse sands when subjected to high heat flux. The speed of the propagating saturation temperature front in partially saturated sands is much higher relative to fully saturated ones due to lesser amount of water available to be heated. In addition, Sundberg (1988) postulated that at higher temperatures and intermediate degrees of saturation, contribution of the vapor diffusion to the effective thermal conductivity increases which could result in the effective thermal conductivity of partially saturated soils being higher than that of the fully saturated soils at temperatures greater than 60 ^{o}C. This also explains why the speed of the propagating saturation temperature front is higher in more permeable partially saturated coarse sand because of the ease of vapor diffusion within the pores of the soil matrix.

4.2.3 Dimensionless Numbers

In the earlier section § 4.2.1, it has been demonstrated that a critical Rayleigh number can be used as a criterion to predict the onset of convection in soil media fully saturated with water, provided that the Boussinesq approximation is valid and the pore water pressure is negligibly small. As a corollary, it is equally critical to measure the relative rate at which heat is transferred through the soil column at the onset of convection compared to pure conduction. Consequently, another dimensionless parameter should be identified to characterize the heat transfer rate with and without convection, in fully saturated soil media when subjected to a high heat flux.

Typically in a boundary layer, the average Nusselt number provides a measure of the convective heat transfer occurring at the surface and is defined as $Nu = hL/k$. Many authors (Nield & Bejan 1999, Bau & Torrance 1982, etc.) have applied the Nusselt number analogously to provide a measure of the increase in heat transport rate at the onset of convection in porous media. Multiplying both the nominator and denominator by ΔT, we get:

$$Nu = \frac{h\Delta T}{\left(\frac{k_{eff}\Delta T}{H}\right)} = \frac{\dot{q}''_{applied}}{\left(\frac{k_{eff}\Delta T}{H}\right)} = \frac{\dot{q}''_{applied}}{\dot{q}''_{conduction}} \qquad (4.11)$$

where h is the overall heat transfer coefficient; k_e is the effect ive thermal conductivity of the soil medium; T is the temperature; H is the height of the intermediate zone; $\Delta T/H$ is the mean linearized temperature gradient across the intermediate zone and $\dot{q}''$ is the heat flux.

Hence, the Nusselt number can be interpreted as a ratio of the applied heat flux to the conduction heat flux in the absence of convection. It is useful as a measure of the relative effectiveness at which heat transfer takes place in the soil medium (i.e. $Nu \geq 1$).

In geotechnics, the definition of the Nusselt number as given by Eqn. (4.11) applies well under steady-state conditions. Typically, $h\Delta T$ encompasses respective heat contributions from conduction and convection only. However, transient conditions with boiling in our experiments complicate the matter and pose the difficulty of

measuring $h\Delta T$ accurately. In our context, $\dot{q}''_{applied}$ is the sum of four heat flux components namely $\dot{q}''_{conduction}$, $\dot{q}''_{convection}$, $\dot{q}''_{boiling}$ and transient parameter $\dot{q}''_{storage}$. In most typical cases, $h\Delta T$ *is* equal to $\dot{q}''_{conduction} + \dot{q}''_{convection} = \dot{q}''_{applied} - \dot{q}''_{boiling} - \dot{q}''_{storage}$. However, $\dot{q}''_{storage}$ and $\dot{q}''_{boiling}$ cannot be measured accurately with the current experimental setup and furthermore, $\dot{q}''_{storage}$ is a transient parameter. It is then hypothesized to define a transient Nusselt number $Nu_{transient}$ such that the overall heat flux applied $\dot{q}''_{applied}$ is treated in a macroscopic fashion. Consequently, we define the nominator in Eqn (4.11) $h\Delta T = \dot{q}''_{applied}$ where $\dot{q}''_{applied}$ is the sum of four heat flux components namely $\dot{q}''_{conduction}$, $\dot{q}''_{convection}$, $\dot{q}''_{boiling}$ and transient parameter $\dot{q}''_{storage}$, and the denominator $\dot{q}''_{conduction}$ is estimated by $k_e\Delta T/H$ where $\Delta T/H$ is the mean linearized temperature gradient across the intermediate zone. Employing the transient Nusselt number $Nu_{transient}$ in a macroscopic fashion will give a *comparative* measure of the effectiveness at which the *overall* heat transfer takes place in a soil medium compared to that by conduction, and avoids the intractable problem of determining transient parameters. It should be noted that the transient Nusselt number will not be equal to 1 for cases without convection because of the presence of boiling phenomena under transient conditions.

Figure 31 shows that there is considerable difference in the values of the transient Nusselt number *Nu* with and without convection in the coarse and fine sand, regardless whether fully or partially saturated. It rises rapidly to around 50~55 at the

onset of convection whereas the values remain relatively steady at 15~20 without convection. Comparing the orders of magnitude, it is inferred that the transient heat transfer rate with convection/boiling is about 2~3 times greater than that by pure conduction/boiling. This is further reinforced by the fact that the average propagating speed of saturated temperature front in fully saturated coarse sand is the same order of magnitude greater than that in fully saturated fine sand. Similar observations can be made from Figure 32 which describes the time variation in Nusselt number when fully saturated coarse sand is exposed to three different levels of heat flux namely low (= 4.4 kW/m^2), moderate (= 12.8 kW/m^2) and high (= 32.6 kW/m^2) heat flux. All these results indicate that when saturated soils are subjected to extreme temperature, the higher the permeability of the saturated soil media, the more likely convection will be generated, and subsequently the greater heat transfer rate (2~3 times greater), notwithstanding the soil temperature will be capped at approximately 100 ^oC (saturation temperature) till dryout of water in the media occur. This behavior is contrary to that of dry soil which shows a gradual temperature rise with time.

Therefore, the types of thermal transport modes occurring in the soil medium, which in turn are affected by the permeability and saturation conditions, appear to be more important factors than the thermal conductivity of the soil skeleton in determining the rate of heating. Furthermore, the propagation speed appears to have a positive correlation with the rate of heat transfer, with higher speed at greater heat transfer rate.

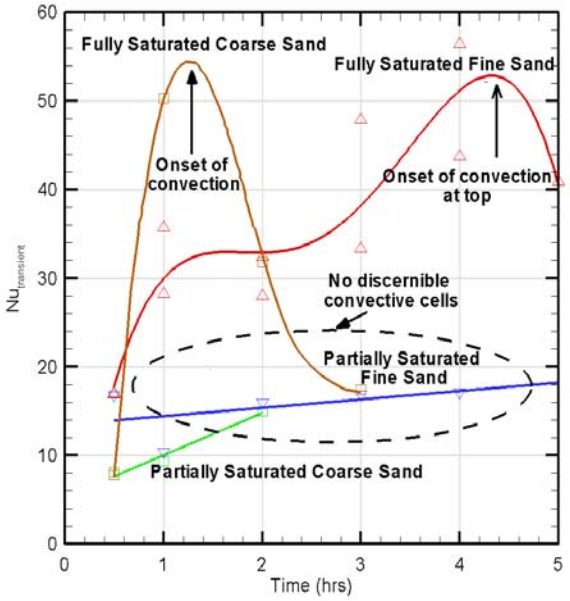

Figure 31. Time variation of transient *Nu* number for fully and partially saturated, coarse and fine sand at high heat flux.

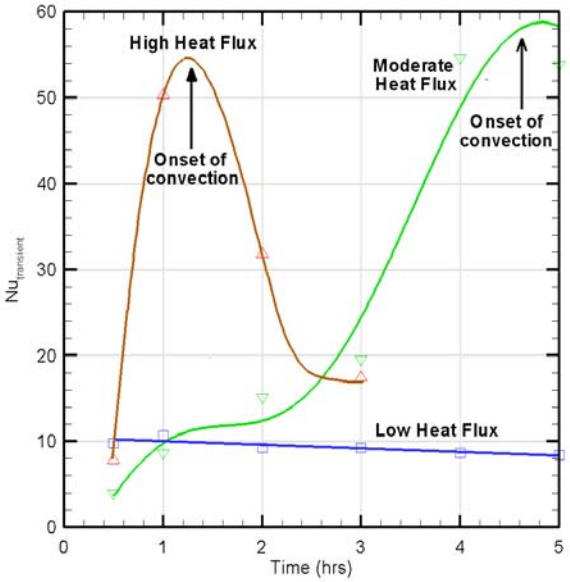

Figure 32. Time variation of the transient *Nu* number for fully saturated coarse soil exposed to different levels of heat flux. High = 32.6kW/m^2; Moderate = 12.8kW/m^2; Low = 4.4 kW/m^2.

4.2.4 Pore Water Pressure in Fully Saturated Silt Subjected to High Heat Flux

Expounded in preceding § 2.3.3, Campanella and Mitchell (1968) derived a simplified expression which could estimate the pore water pressure under undrained conditions based on several factors. Eqn. (2.42) is described as follows:

$$\Delta P = \frac{\phi \, \Delta T \, (\beta_s - \beta_w) + \beta_{st} \Delta T}{m_v}$$

Alternatively, since the pore pressure parameter F is relatively constant for a wide range of effective stress, Mitchell suggested that this parameter F could be used to estimate the pore water pressure. Since pore water in the saturated silt matrix cannot be drained as freely compared to that in the fully saturated coarse or fine sand, it is reasonable to assume that pore water pressure in saturated silt matrix will build up in accordance to undrained condition. Substituting the values F = 0.044/^{o}F (saturated sandstone), ΔT = 212 ^{o}F(= 100 ^{o}C) – 77 ^{o}F(= 25 ^{o}C) = 135 ^{o}F, σ_{eff} = 0.084 kg/cm^2, we get:

$$F = \frac{\frac{\Delta P}{\Delta T}}{\sigma_{eff}} \Rightarrow \frac{\Delta P}{\sigma_{eff}} = \text{F x } \Delta\text{T}$$

$$\Rightarrow \frac{\Delta P}{\sigma_{eff}} = 0.044\text{x}135 = 5.94 \text{ (about 500\% overpressure)}$$

$$\Rightarrow \Delta\text{P} = \text{F x } \Delta\text{T x } \sigma_{\text{eff}}$$

$$= 0.044 \text{ x } 135 \text{ x } 0.084$$

$$\approx 0.5 \text{ kg/cm}^2 = 50 \text{ kPa}$$

It can be seen that the predicted excess pore water pressure is in the same order of magnitude with the experimental values (25~40kPa) in silts which validates this qualitative approach. In addition, this tremendous overpressure of about 500%, over and above the overlaying load stress, built up in the soil medium exposed to high heat flux, warrants serious consideration during tunnel design and construction. Appropriate safety factors used for the construction of tunnels should take into account the effect of this potential overpressure arising from tunnel fires. It should also be kept in mind that a higher effective stress will engender greater change in pore water pressure for a given temperature change. As a result, the pore water pressure developed during a tunnel fire could be substantial and be a concern for tunnels that have significant depth of overlaying soils weighing above them.

4.2.5 Consolidation and Peak Strength Effect on Soils At Elevated Temperature

Excavation of the silt indicates that some consolidation develops during the heating process, which in turn is likely to lead to increased peak strength of the soil structure, although that densification is not quantified in these experiments. Previous torvane shear strength measurements (Capka 2004) for silt specimens taken at 80 mm height after heating, produced values from 25 to 35 kPa which are far greater than that of the silt slurry before heating. Campanella and Mitchell (1968) reported similar densification behavior in their experiments on clay soils heated to cooler temperatures, not exceeding 60^{o}C. They hypothesized that when saturated soil is heated and expands, the particles themselves do not expand measurably, however the water in the pores does. This accounts for the increase in pore water pressures

observed. Dissipation of pore water pressures while the soil is hot leads to flow of water from the pores although the pores are believed to remain saturated. Note that permeability will increase because heating the water decreases its viscosity. When the still saturated soil cools, the pore water contracts in volume and will lead to a reduction in pore water pressure that leads to thermally induced consolidation when soil permeability is low, as in the case of silt. This same behaviour was reported by Houston et al. (1985) based on their experiments on silt heated to a maximum of 200^{o}C in the triaxial apparatus. This phenomenon will be investigated in forthcoming experiments.

Partially saturated silt experiments are not described here, as it was not possible to prepare repeatable specimens with that condition.

Furthermore, it is postulated that the higher pore water pressure built up in the silt column is likely to cause some soil migration since the silt particles are relatively much finer (200 ~ 600%) compared to that of coarse and fine sands.

On the other hand, there is no strong evidence to suggest that there is any apparent consolidation/compression effect or peak strength augmentation when fully saturated coarse and fine sands are heated. Furthermore, no significant movement of dyed sand, placed strategically within the soil column, suggests that the increase in the pore water pressure is not considerable to result in soil migration when heated.

4.2.6 Formation of Void Channels at Soil/Tunnel Interface

Some researchers have reported that vaporization of water in porous media during boiling can create void channels through which the vapor escapes (Eckert et al. 1985, Reed 1986). We observed this phenomenon in a separate experiment conducted using a pyrex glass filled with saturated soils in which void channels were noted at the pyrex glass/soil interface. Development of higher pore pressures in finer-grained soil of low permeability could further enhance this phenomenon. Since continuous contact between a tunnel lining and the soil surrounding the tunnel is considered to be important to tunnel integrity (Tunnel Engineering Handbook, 1996), a cycle that includes the development of high water pressures, relieved suddenly by the formation of void channels, followed by further development of high water pressures, may have a further negative effect on tunnel integrity during a fire. If there is no continuous contact between the lining and the surrounding soil medium i.e. existence of voids, to provide support for the tunnel, it may lead to large uncontrolled deformation of the tunnel lining due to unsupported section. Figure 33 depicts the two possible adverse soil/tunnel interaction scenarios that could be expected as a result of extreme heat from tunnel fires.

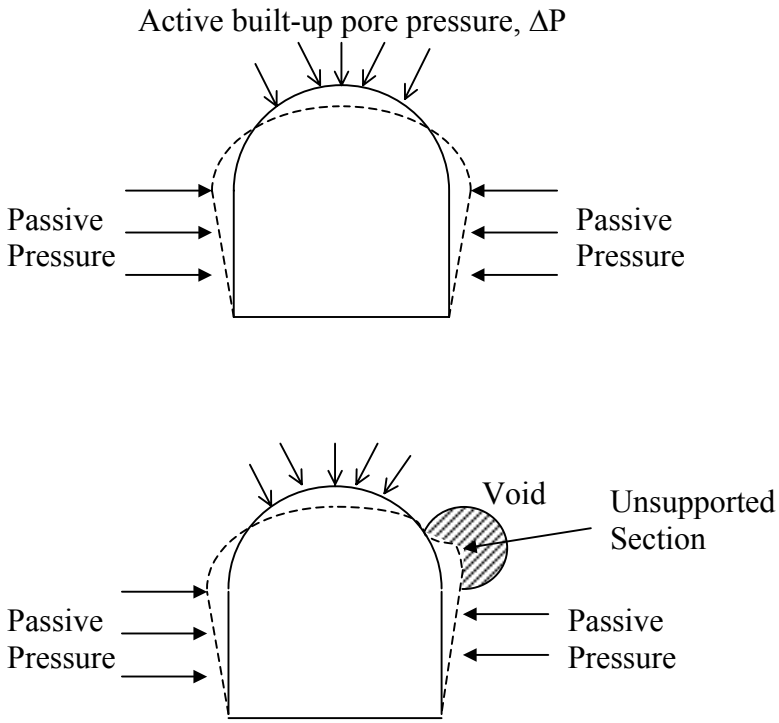

Figure 33. Possible adverse soil/tunnel interaction scenarios due to extreme heating from tunnel fires.

CHAPTER 5: CONCLUSIONS

The main findings of this exploratory project are summarized below:

(1) It is found that the behavior of dry soil subjected to extreme heating in the experimental soil column configuration follows closely that of a semi-infinite 1-D heat transfer model with a fixed surface temperature applied at the bottom. An analytical model based on 1-D heat transfer has been developed and there is good agreement between the actual and predicted behaviors;

(2) When water is present in the soil, temperature in the water-saturated soils never exceed saturation temperature ($\approx 100^{o}C$) even when exposed to high heat flux, until dryout of water occurs after prolonged heating;

(3) In fully saturated soils, the onset of convection cells happens in soil of higher permeability. This accelerates the transient heat transfer process (2~3 times) substantially compared to heat transfer by pure conduction/boiling. Therefore, the types of thermal transport modes occurring in the soil medium, which in turn is affected by the permeability and saturation conditions, appear to be more important factors than the thermal conductivity of the soil skeleton in determining the rate of heating. Furthermore, there is propagation of a saturation temperature front through the soil column at the onset of boiling, with greater propagation speed measured in more permeable coarse sand. The propagation speed is also found to have a positive correlation with the rate of heat transfer, with higher speed at greater heat transfer rate;

(4) There is significant increase in the pore water pressure building up in finer-grained saturated soil with low permeability when heated. This overpressure of about 500%, over and above the overlaying load stress, built up in the silt when heated, warrants serious consideration during tunnel design and construction. In addition, the appreciably higher pressure measured in silts may be responsible for driving the onset of convection, which typically would not be generated by buoyancy-induced forces;

(5) It is found that the modified transient Rayleigh number can be used as a criterion to reasonably predict the onset of convection in saturated soils when the Boussinesq assumption is applicable. However, when the pore water pressure is appreciably high such as in silts to cause probable soil migration, this predictive method is no longer valid. Furthermore, the transient Nusselt number is found to be useful as a measure of the relative effectiveness at which heat transfer takes place in the soil medium;

(6) When a soil has low permeability and is fine-grained e.g. silt, effects such as consolidation and higher peak strength appear to develop when heated. Furthermore, the higher resulting pore water pressure is likely to cause significant soil migration which could be detrimental to stability of tunnel lining;

(7) The type of soil overlaying the tunnel lining will determine the type of thermal transport mechanisms occurring in the soil medium, which in turn will affect the rate at which the heat is drawn from the fire. A higher heat transfer rate due to convection and boiling will remove the heat from the tunnel fires

more quickly and produces an adverse temperature gradient across the tunnel lining, which is known to aggravate thermally-induced degradation effects in the lining such as spalling in concrete; and

(8) The integrity of tunnel lining during a fire has hitherto considered only the built-up pore pressure within the concrete and ensuing spalling effects. However, higher pore pressure may enhance the creation of void channels in which the vapor escapes, thus increasing the chance of producing a region of discontinuity (unsupported section) at the surrounding soil/tunnel lining interface that could affect adversely the stability of the tunnel lining. Furthermore, there is a possibility of additional unwanted pressure (~500%) from the supporting soil structure acting on the tunnel lining which contributes adversely to the stresses experienced by the tunnel lining during a severe fire.

The major observations of the soil response subjected to extreme heating for different soil type and saturation conditions are summarized in Table 6.

Table 6. Summary of the soil behaviors subjected to extreme heating for the different soil type and saturation conditions

Type of Soil	Main Heat Transfer Mechanisms	Speed of saturation temperature front	Excess pore water pressure	Any permanent densification?	Peak Strength	Any Soil Migration /Channeling?
Dry Soil	Conduction only	NA	~ 1kPa	No apparent change	No significant increase	No apparent soil channeling
Fully Saturated Sands	Conduction & Boiling Convection for coarse sand only	300~400mm/hr (coarse) 100~200mm/hr (fine)	2~8 kPa (coarse) 7~14kPa (fine)	No apparent change	No significant increase	Soil channeling
Partially Saturated Sands	Conduction & Boiling No Convection	400~500mm/hr (coarse) 200~300mm/hr (fine)	2~8 kPa (coarse) 7~14kPa (fine)	No apparent change	No significant increase	Soil channeling
Silt	Conduction & Boiling More Vigorous Convection	Onset of boiling occurs throughout the silt column simultaneously	25~40kPa	Permanent densification	Increase	Soil channeling and likely soil migration

CHAPTER 6 : RECOMMENDATIONS

The first exploratory phase of this research has provided specific results that vindicate real concerns for the potential adverse geotechnical effect on the stability of the tunnel lining. Ultimately, it is envisaged that this research may provide the impetus to increase the safety factor typically used in the design and construction of tunnel lining to take into account these geotechnical effects arising from tunnel fires. However, more in-depth studies need to be done and some ideas are put forth to identify future directions and areas of focus for the research:

(1) Albeit response of dry soil to extreme heat has been well-modeled, existing established methods developed assuming steady-state conditions are inadequate to describe the response of water-saturated soil to transient-state conditions, which are a better representation of the actual ground conditions encountered in tunnel fires. Therefore, with the database of experimental results on the geotechnical response subjected to extreme heat being established, it is imperative that future studies should focus on developing an analytical model using finite element method to predict the transient-state geotechnical response in terms of pore pressure and temperature distribution. The theoretical results generated should then be compared against the experimental results to evaluate the predictive capabilities of the model. Once this model is developed, it will be an extremely useful tool to help in assessing the impact on the surrounding ground support accurately during severe tunnel fires for a myriad of different boundary conditions and soil types.

(2) It is further suggested that more experiments should be run to measure the response of a greater variety of different soil types such as partially and fully saturated clay subjected to extreme heat. This will not only help to further verify whether the qualitative hypothesis proposed in this thesis are applicable in other soil types, at the same time, expands the experimental database to evaluate the results of the analytical model for great diversity of different soil types.

(3) It has been found that as the permeability of soils decreases, the changes in soil compressibility and strength become increasingly important in the soil behaviors exposed to elevated temperature. For example, it has been found that soil compressibility will affect the development of pore water pressure with increasing temperature. After the experimental database on an overall system level has been established, it makes sense now to conduct experiments to measure dependence of soil compressibility and strength variation of smaller specimens with increasing temperature in greater details, similar to those performed by Houston et al. (1985).

(4) It is envisaged that actual fire tests on a scaled tunnel-soil medium model representative of the actual tunnel geometry, should be run in the future so that the experimental results can be assessed against that predicted by the analytical model.

Appendix A: Calculations of Effective Thermal Conductivity of Soil Medium

If heat conduction in the porous medium occurs in parallel, the thermal conductivity of the soil medium is given by:-

$$k_{PL} = (1-\phi)k_s + \varphi k_f$$

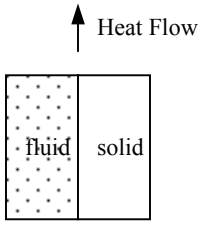

If heat conduction in the porous medium occurs in series, the thermal conductivity of the soil medium is given by:-

$$\frac{1}{k_{SR}} = \frac{1-\varphi}{k_s} + \frac{\varphi}{k_f}$$

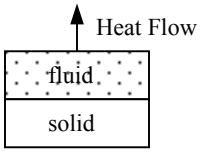

Obviously, the effective thermal conductivity k_{eff} must lie between k_{sr} and k_{pl}.

For fully saturated fine sand, $\phi \approx 0.38 \sim 0.4$, k_s= 7 W/m.K and k_f = 650x10^{-3} W/m.K (at T=330K)

$$\left(\frac{1-0.4}{7} + \frac{0.4}{650\times10^{-3}}\right)^{-1} < k_{eff} < (1-0.4)\times 7 + 0.4\times 650\times 10^{-3}$$

$\Rightarrow 1.43 < k_{eff} < 4.5 \Rightarrow k_{eff}$(average) $\approx$ 3 W/m-K

For fully saturated coarse sand, $\phi \approx 0.48 \sim 0.5$

$$\left(\frac{1-0.5}{7} + \frac{0.5}{650\times10^{-3}}\right)^{-1} < k_{eff} < (1-0.5)\times 7 + 0.5\times 650\times 10^{-3}$$

$\Rightarrow 1.2 < k_{eff} < 3.8 \Rightarrow k_{eff}$(average) $\approx$ 2.5 W/m-K

Appendix B: Procedures to Set Up the Test Apparatus and Prepare the Soil Column

The step-by-step procedures for the setting up of the test apparatus and preparation of the soil column are described below:

1. Assemble the 3 components of the testing tube using rivets and apply adequate amount of the RTV silicone uniformly onto the joints;
2. Once the RTV silicone is air-dried, secure the joints with the tube clamps to provide a tight water seal;
3. Insert the SS pipes for the pressure transducers and the pressure gauges into the swagelok fittings attached to the tube;
4. Mount the testing tube securely to the frame;
5. Bolt the thermocouple (OMEGA Part # XCIB-K-4-1-3) to the bottom of the testing tube;
6. Insert the array of 16 integrated thermocouples into the swagelok fittings. The ends of the stainless steel pipes holding the thermocouples (Omega Part# GG-K-36-SLE-200) outside the tube are then clamped using copper split-bolt connectors and sealed with RTV silicone to prevent water leakage.;
7. Then connect the thermocouple wires to the NetDAQ data acquisition unit using the quick-connect connectors accordingly;
8. Wrap the glass-wool insulation around the testing tube and tighten with clamps;
9. The sand raining method is often used in sand placement experiments to achieve a highly uniform density sand sample. Fill the testing tube with sand

slowly, raining it through a sieve, until the 16th thermocouple (about 1200 mm from the bottom) is buried under the sand. The meshes forming the sieve are roughly equivalent to the U.S. Standard Sieve No. 20. Minimum and maximum dry unit weight tests are performed for the fine sand to determine the density variation throughout the sand column in order to check uniform density distribution.

10. Attach the pressure transducers and the pressure gauges to the SS pipes; The pressure transducers are already pre-connected to the NetDAQ data acquisition unit;
11. For experiments involving fully saturated sands, water is added to the sand from the bottom of the testing tube via the bottom valve, until the water level exceeds the top of the sand column.
12. Position the heater centrally about 4" below the testing tube;
13. Insert another thermocouple into the thermal well of the heater and connect the wire to the temperature controller which will regulate its surface temperature to about 750^{o}C.
14. The tests involving silt are prepared and performed in a different manner than the sand tests principally because of difficulties in placing a uniform saturated specimen of silt. Silt is first mixed with water in a bowl and stirred well to achieve a fully uniform saturation. The moisture content of the silt is set to approximately 33% mass of volume. After thorough mixing, the fully saturated silt is placed carefully into the testing tube up to the elevation of the

10th thermocouple (about 254 mm from the bottom). The column between the 10th and 16th thermocouples is filled with fully saturated fine sand;

15. The regulated power supply powering the pressure transducers are switched on;
16. The NetDAQ data acquisition program in the PC is put on standby mode, ready to collect data for the experiment.

Appendix C: ASTM Standard Test Method for Laboratory Determination of Water (Moisture) Content of Soil and Rock by Mass

Immediately after the specimens at different elevations are collected, the container and test specimens are weighed to obtain M_{cws} and M_c. The test specimens are then dried in an oven at a constant temperature of 110° ± 5°C till the mass remains unchanged, yielding M_{cds}. The loss of mass due to drying is attributed to the loss of water. The residual water content is calculated using the mass of water lost and the mass of the dry specimen and is shown as follows:

$$w = [(M_{cws} - M_{cs})/(M_{cs} - M_c)] \times 100 = \frac{M_w}{M_s} \times 100$$

where

w = residual water content, %

M_{cws} = mass of container and wet specimen, g,

M_{cds} = mass of container and dry specimen, g,

M_{cs} = mass of container and oven dry specimen, g,

M_c = mass of container, g,

M_w = mass of water lost ($M_w = M_{cws} - M_{cds}$), g, and

M_s = mass of solid particles ($M_s = M_{cds} - M_c$), g

BIBLIOGRAPHY

1. ASTM, 2002, "Annual Book of ASTM Standards, Section 4-Construction", Volume 04.08 Soil and Rock (I): D 420 – D 5779.

2. Bau, H. and Torrance, K.E., 1982, "Boiling in Low Permeability Porous Materials", International Journal of Heat Mass Transfer, Vol. 25, No. 1, pp 45-55.

3. Bau, H. and Torrance, K.E., 1982, "Low Rayleigh Number Thermal Convection in a Vertical Cylinder Filled with Porous Materials and Heated from Below", ASME Journal of Heat Transfer, Vol. 104, pp 166-172.

4. Campanella, R.G. and Mitchell, J.K., 1968, "Influence of Temperature Variations on Soil Behaviour", Vol. 49, No. SM3, ASCE, pp709-734.

5. Capka, D., May 2004, "Response of Soil to High Temperatures", MSc Research Paper, School of Civil & Environmental Engineering, University of Maryland.

6. Carslaw, H.S. and Jaeger, J.C., 1986, "Conduction of Heat in Solids", 2nd Ed, Oxford University Press.

7. Eckert, E. R. G., Goldstein, R. J., Behbahani, A. I. and Hain, R., 1985, "Boiling in an Unconsolidated Granular Medium", International Journal of Heat Mass Transfer, Vol. 28, pp 1187-1196.

8. Eckert E.R. and M. Faghri, 1980, "A General Analysis of Moisture Migration Caused by Temperature Differences in An Unsaturated Porous Medium", Int. Journal of Heat Mass Transfer, Vol. 23, pp 1613-1623, Pergamon Press Ltd, Great Britain.

9. Elder, J.W., 1967, "Steady Free Convection in a Porous Medium Heated from Below", Journal of Fluid Mechanics, Vol. 27, pp29-48.

10. French Task Force, 30 June 1999, "Report for the Technical Investigation of the 24 March 1999 Fire in the Mont Blanc Vehicular Tunnel", Ministry of Interior, France.

11. Gehrig, D., Feb 2004. “Extreme heat Geotechnics”, Attachment Report, University of Maryland.

12. Green S.L., 1984, “The Behavior of Deep Ocean Sediments in Response to Thermo-Mechanical Loading”, Ph.D. thesis, University of California, Berkeley.

13. Highway Research Board, 1969, “Effects of Temperature and Heat on Engineering Behavior of Soils”, Special Report 103, Proceedings of an International Conference, Washington D.C.

14. Horton, C.W. and Rogers, F.T.Jr., 1945, “Convection Currents in a Porous Medium”, Journal of Applied Physics, Vo1. 16, pp367-370.

15. Houston, S.L. and Lin, H-D, 1987, “A Thermal Consolidation Model for Pelagic Clays”, Journal of Marine Geotechnology, Vol. 7, pp 79-98.

16. Houston, S.L., Houston, W.N. and Williams, N.D., 1985, “Thermo-Mechanical Behavior of Seafloor Sediments”, Journal of Geotechnical Engineering, ASCE, Vol. 111, No. 11, pp1249-1263.

17. Howle, L.E., Behringer, R.P. and Georgiadis, J.G., 1997, “Convection and Flow in Porous Media. Part 2. Visualization by shadowgraph”, Journal of Fluid Mechanics, Vol. 332, pp 247-262.

18. Incropera, F.P. and DeWitt, D.P., 1985, “Fundamentals of Heat and Mass Transfer”, 2nd Ed, John Wiley and Sons, New York.

19. Joe, M. S. and Schubert G., 1977, “Thermal Convection of Water in a Porous Medium: Effects of Temperature- and Pressure-Dependent Thermodynamics and Transport Properties”, Journal of Geophysical Research, Vol 82, No. 2, pp325-333.

20. Johansen, O., 1975, “Thermal Conductivity of Soils”,Ph.D. Dissertation, Trondheim, Norway, ADA 044002.

21. John, O.B., Thomas, R.K. and Elwyn, H.K. (Editors), 1996, "Tunnel Engineering Handbook", 2nd Edition, Chapman & Hall, NY.

22. Katto, Y. and Masuoka, T., 1967, "Criterion for the Onset of Convective Flow in a Fluid in a Porous Medium", Int. Journal of Heat Mass Transfer, Vol. 10, pp 297-309.

23. Laguros, J.G., 1969, "Effects of Temperature on Some Engineering Properties of Clay Soils", Proc of Int. Conference on Effects of Temperature and Heat on Engineering Behavior of Soil, National Research Council, HRB, Washington D.C., pp 186-193.

24. Lapwood, E.R., 1948, "Convection of a Fluid in a Porous Medium", Proceedings of Cambridge Phil. Soc., Vol. 44, pp508-521.

25. Lin, H-D., 1985, "A Study of Thermally Induced Time-Dependent Canister Migration", Ph.D. thesis, University of California, Berkeley.

26. McGrattan, K. and Hamins, A., 2003, "Numerical Simulation of the Howard Street Tunnel Fire, Baltimore, Maryland, July 2001", NISTIR 6902, National Institute of Standards and Technology, Gaithersburg, MD.

27. Mitchell, J.K., 1993, "Fundamentals of Soil Behaviour", 2nd Edition, John Wiley & Sons Inc, NY.

28. Mitchell, J.K., 1969, "Temperature Effects on the Engineering Properties and Behaviour of Soils", Proc of Int. Conference on Effects of Temperature and Heat on Engineering Behavior of Soil, National Research Council, HRB, Washington D.C., pp 9-28.

29. Nield, D.A., 1968, "Onset of Thermohaline Convection in a Porous Medium", Water Resources Research, Vol. 4, No. 3, pp553-559.

30. Nield, D.A. and Bejan, A., 1999, "Convection in Porous Media", 2nd Ed, Springer-Verlag New York Inc.

31. Paul K., Oct 2004. “Extreme heat Geotechnics II”, Attachment Report, University of Maryland.

32. Ramesh, P.S. and Torrance, K.E., 1990, “Stability of Boiling in Porous Media”, Int. Journal of Heat Mass Transfer, Vol. 33, No. 9, pp 1895-1908.

33. Reed, A.W., 1986, “A Mechanistic Explanation of Channels in Debris Beds”, ASME, Journal of Heat Transfer, Vol. 108, pp 125-131.

34. Sahota, M.S. and Pagni, P.J., 1979, “Heat and Mass Transfer in Porous Media Subject to Fires”, Int. Journal of Heat Mass Transfer, Vol. 22, pp 1069-1081.

35. Sattuck, M.D., Behringer, R.P., Johnson, G.A. and Georgiadis, J.G., 1997, “Convection and Flow in Porous Media. Part 1. Visualization by Magnetic Resonance Imaging”, Journal of Fluid Mechanics, Vol. 332,pp 215-245.

36. Schubert, G. and Straus, J.M., 1980, “Gravitational Stability of Water Over Steam in Vapor-Dominated Geothermal System”, Journal of Gephysical Research, Vol. 85, pp 6505-6512.

37. Sherif, M. and Burrous, C.M., 1969, “Temperature Effects on the Unconfined shear Strength of Saturated Cohesive Soil”, Proc of Int. Conference on Effects of Temperature and Heat on Engineering Behavior of Soil, National Research Council, HRB, Washington D.C., pp 267-272.

38. Sundberg, J., 1988, “Thermal Properties of Soils and Rocks”, Report No. 35, Swedish Geotechnical Institute.

39. Tan, K.K. and Thorpe, R.B., 1996, “The Onset of Convection Caused by Buoyancy During Transient Heat Conduction in Deep Fluids”, Vol. 51, No. 17, pp4127-4136.

40. Terzaghi, K., October 1925 “Simplified Soil Tests for Subgrades and Their Physical Significance” Public Roads.

41. Ulm, F. J., Coussy, O. and Bazant, Z.P., March 1999a, “The Chunnel Fire I – Chemoplastic Softening in Rapidly Heated Concrete”, Journal of Engineering Mechanics, ASCE, 125(3), pp 272-282.

42. Ulm, F. J., Acker, P. and Levy, M., March 1999b, “The Chunnel Fire II – Analysis of Concrete Damage”, Journal of Engineering Mechanics, ASCE, 125(3), pp 283-289.